Fast Multiscale Gaussian Beam Methods for Wave Equations in Bounded Convex Domains

Gang Bao[*]   Jun Lai[†]   Jianliang Qian[‡]

Abstract

Motivated by fast multiscale Gaussian wavepacket transforms and multiscale Gaussian beam methods which were originally designed for pure initial-value problems of wave equations, we develop fast multiscale Gaussian beam methods for initial boundary value problems of wave equations in bounded convex domains in the high frequency regime. To compute the wave propagation in bounded convex domains, we have to take into account reflecting multiscale Gaussian beams, which are accomplished by enforcing reflecting boundary conditions during beam propagation and carrying out suitable reflecting beam summation. To propagate multiscale beams efficiently, we prove that the ratio of the squared magnitude of beam amplitude and the beam width is roughly conserved, and accordingly we propose an effective indicator to identify significant beams. We also prove that the resulting multiscale Gaussian beam methods converge asymptotically. Numerical examples demonstrate the accuracy and efficiency of the method.

Keywords: Wave equation, multiscale Gaussian beam, bounded domain, high-frequency wave

1   Introduction

We consider the following initial-boundary value problem (IBVP) of the wave equation,

$$\begin{cases} u_{tt} - V^2(x)\Delta u = 0, \quad x \in D, \quad t > 0, \\ \quad u(x,t)|_{t=0} = f_1(x), \\ \quad u(x,t)_t|_{t=0} = f_2(x), \\ \quad u(x,t)|_{x \in \partial D} = 0, \end{cases} \tag{1}$$

where D is a convex bounded domain in $\mathbb{R}^d$, and the velocity $V(x)$ is smooth, positive and bounded away from zero. Compared to the slowly changing velocity function, initial conditions $f_1(x) \in H^1(D)$ and $f_2(x) \in L^2(D)$ are assumed to be highly oscillatory, compactly supported functions.

Since the initial oscillations result in high-frequency waves, direct methods such as finite-difference or finite-element methods require a large number of grid points to resolve highly oscillatory solutions, and the resulting computational cost is overwhelmingly high. Consequently, alternative methods such as geometrical-optics based asymptotic methods are

[*]Department of Mathematics, Zhejiang University, Hangzhou 310027, China; Department of Mathematics, Michigan State University, East Lansing, MI 48824. Email: **bao@math.msu.edu**

[†]Department of Mathematics, Michigan State University, East Lansing, MI 48824. Email: **laijun@msu.edu**

[‡]Department of Mathematics, Michigan State University, East Lansing, MI 48824. Email: **qian@math.msu.edu**

sought to compute such high-frequency wave phenomena. One of the powerful geometrical-optics methods is the Gaussian beam method [1, 15, 18, 21], which is able to treat caustics automatically. In this paper, motivated by the work in [17] which designed fast multiscale Gaussian wavepacket transforms and multiscale Gaussian beam methods for pure initial value problems of wave equations, we propose to develop fast multiscale Gaussian beam methods for wave equations in bounded convex domains.

Although Gaussian-beam based numerical methods are well developed for pure initial value problems of Schrödinger equation and wave equations [10, 21, 8, 20, 9, 16, 17, 13, 22, 19, 11], it seems that no efficient numerical Gaussian beam method has been developed for wave equations and Schrödinger equations in bounded domains. In the case of wave equations in bounded domains, some essential difficulties arise in developing numerical Gaussian beams. The first difficulty is that one needs to take care of reflected beams. Theoretically, how to construct reflecting beams has been first addressed in [18] and further detailed in [3]; numerically, we propose a method-of-images based approach to superpose reflected beams so as to enforce homogeneous Dirichlet boundary conditions.

The second one is that a bounded domain of general geometry may give rise to diffraction phenomena or gliding rays along the boundary in the sense of geometrical optics. Since geometrical-optics based approaches including Gaussian beams are not able to capture those effects, other theories, such as geometrical theory of diffraction, Fourier-Airy integrals, or gliding beams, are needed. Therefore, to avoid those potential issues, we will assume that the domain is strictly convex and non-grazing hypothesis [18] holds, and the latter will be satisfied when the initial data is compactly supported away from the boundary.

The third one is how to decompose arbitrary non-periodic initial data into multiscale Gaussian wavepackets. Since the original fast multiscale Gaussian wavepacket transform is designed for periodic functions, we propose to first carry out odd periodic continuations of the initial data, then apply the multiscale Gaussian wavepacket transform to the resulting continued data, propagate and superpose reflecting Gaussian beams in the original domain, and finally extract the beam solution in the original bounded convex domain.

The fourth one is how to identify significant beams so that beam propagation can be carried out more efficiently. We prove that the ratio of the squared magnitude of beam amplitude and the beam width is roughly conserved for each individual beam, and this ratio can be used as an indicator to identify significant beams. This way the number of propagated beams is significantly reduced.

1.1 Related work

The idea underlying Gaussian beams is simply to build asymptotic solutions to partial differential equations concentrated on a single curve through the domain; this single curve is nothing but a ray as shown in [18]. The existence of such solutions has been known to the pure mathematics community since sometime in the 1960s [1], and these solutions have been used to obtain results on propagation of singularities in hyperbolic PDEs [18]. An integral superposition of these solutions can be used to define a more general solution that is not necessarily concentrated on a single curve. Gaussian beams can be used to treat pseudo-differential equations in a natural way, including Helmholtz and Schrödinger equations [10, 21, 8, 20, 9, 16, 17, 13, 19, 11].

Gaussian beam superpositions have been used in geophysical applications for seismic wave modeling [4] and migration [6]. The numerical implementations in these areas are based on ray-centered coordinates which prove to be computationally inefficient [4, 6]. More recently, based on [18, 21] the first Eulerian Gaussian beam method was proposed in [10] which overcomes some of these difficulties; it can be easily applied to both high frequency waves and semi-classical quantum mechanics [8, 9]. In [21] Lagrangian Gaussian beams are successfully constructed to simulate mountain waves, a kind of stationary gravity wave forming over mountain peaks and interfering with aviation.

Based on Ralston [18], [3] analyzed a single-scale Gaussian beam method for initial boundary value problems of wave equations, and the resulting method can handle only single-frequency data. Although our method also heavily relies on [18], ours can handle multiple-frequency data, and we have named it the multiscale Gaussian beam method as it is based on fast multiscale Gaussian wavepacket transforms [17].

A PDE boundary value problem seeks the solution of a PDE with given boundary data; a PDE interface problem can be viewed as a special boundary value problem with an interior boundary such that the solution has a specified jump across the interior boundary. In this regard, single-scale Gaussian beam methods have been derived to take care of interface conditions; for example, see [14] for wave equations and [23] for 1-D Schrödinger equations. On the other hand, the multiscale Gaussian beam method proposed here is for wave equations in bounded convex domains and is able to handle multiple-frequency data.

1.2 Contents

The rest of the paper is organized as follows. Section 2 introduces the Gaussian beam method applied to the wave equation posed in a bounded domain. In Section 3, we briefly review the fast multiscale Gaussian wavepacket transform and its application to the wave equation, details of which can be found in [17]. Section 4 gives the strategy on how to select significant beams and addresses some other numerical issues related to bounded domains. Section 5 proves the asymptotic convergence of the new method. Numerical results are provided in Section 6 to demonstrate the effectiveness of the new method.

2 Gaussian beam methods for the wave equation

2.1 Gaussian beams for initial value problems

We start from the initial value problem of the scalar wave equation in $\mathbb{R}^d$:

$$u_{tt} - V^2(x)\Delta u = 0, \quad x \in \mathbb{R}^d, \ t > 0, \tag{2}$$

where $V(x)$ is smooth, positive and bounded away from zero. Initial conditions $u(0,x) = f_1(x) \in H^1(\mathbb{R}^d)$ and $u_t(0,x) = f_2(x) \in L^2(\mathbb{R}^d)$ are highly oscillatory functions.

We are looking for asymptotic solutions of the wave equation in geometrical-optics form,

$$A(x,t)e^{\imath\omega\tau(x,t)}, \tag{3}$$

where $\tau(x,t)$ is the phase function, $A(x,t)$ the amplitude function, and $\imath = \sqrt{-1}$. In the ansatz (3), the frequency ω is a large parameter, and an asymptotic solution for the wave equation is sought in the sense that the wave equation (2) and its associated initial conditions are satisfied approximately with a small error when ω is large. Substituting the ansatz (3) into the wave equation (2) and considering the leading orders in inverse powers of the large parameter ω, we end up with the following eikonal and transport equations:

$$\tau_t^2 - V^2(x)|\nabla_x\tau(x,t)|^2 = 0, \tag{4}$$
$$2A_t\tau_t - 2V^2\nabla_x A \cdot \nabla_x\tau + A(\tau_{tt} - V^2\text{trace}(\tau_{xx})) = 0. \tag{5}$$

Factorizing the eikonal equation (4) gives

$$\tau_t^\pm + G^\pm(x, \nabla_x\tau(x,t)) = 0, \tag{6}$$

where $G^\pm(x, \nabla_x\tau(x,t)) = \pm V(x)|\nabla_x\tau(x,t)|$ correspond to two polarized wave modes in the second-order wave equation. Accordingly, we define the Hamiltonians,

$$G^\pm(x,p) = \pm V(x)|p|,$$

3

where $G^{\pm}(x, p)$ is clearly homogeneous of degree one in the momentum variable p.

To construct asymptotic solutions for the wave equation, we are going to use Gaussian beams [18, 12, 21]. Because the two polarized wave modes will be treated essentially in the same way, we consider the following generic situation for the eikonal equation:

$$\tau_t + G(x, \nabla_x \tau(x, t)) = 0, \tag{7}$$

where G can be taken to be either G^+ or G^- and τ to be either τ^+ or τ^-. According to the Gaussian beam theory [18, 12, 21], a single Gaussian beam is an asymptotic solution to the wave equation, and it is concentrated near a ray path which is the x-projection of a certain bicharacteristic. To construct a bicharacteristic, we apply the method of characteristics to the eikonal equation (7) to obtain the following Hamiltonian system:

$$\dot{x} = \frac{dx}{dt} = G_p, \quad x|_{t=0} = x_0, \tag{8}$$

$$\dot{p} = \frac{dp}{dt} = -G_x, \quad p|_{t=0} = p_0, \tag{9}$$

where t is time parameterizing bicharacteristics. Solving this system yields the bicharacteristic

$$\{(x(t), p(t)) : t \geq 0\},$$

which emanates from the initial point (x_0, p_0) in phase space at $t = 0$. The corresponding ray path is $\gamma = \{(x(t), t) : t \geq 0\}$, which is defined in the (x, t)-space. Notice that along the ray path $\gamma = \{(x(t), t) : t \geq 0\}$, we have by construction $p(t) = \tau_x(x(t), t)$ due to the method of characteristics. Furthermore, the phase function $\tau(x(t), t)$ along the ray path satisfies

$$\frac{d\tau(x(t), t)}{dt} = \tau_t(x(t), t) + p(t) \cdot G_p(x(t), p(t)) = \tau_t(x(t), t) + G(x(t), \tau_x(x(t), t)) = 0,$$

which implies that the phase function $\tau(x(t), t)$ does not change along γ because the Hamiltonian G is homogeneous of degree one; we will take $\tau(x(t), t) = 0$.

So far we have computed the phase function τ and its first-order derivative $p(t) = \tau_x(x(t), t)$ along the ray path $\gamma = \{(x(t), t) : t \geq 0\}$. To construct a second-order Taylor expansion for the phase function along the ray path, one needs to compute the Hessian of the phase along the ray. Following [18, 21], we differentiate the eikonal equation (7) with respect to t and x near the ray path γ:

$$\tau_{t,x}(x, t) + G_x(x, \tau_x(x, t)) + \tau_{xx}(x, t) G_p(x, \tau_x(x, t)) = 0, \tag{10}$$

$$\tau_{t,t}(x, t) + G_p(x, \tau_x(x, t)) \cdot \tau_{x,t}(x, t) = 0. \tag{11}$$

Differentiating equation (10) further with respect to x yields the following Riccati equation for $M(t) = \tau_{xx}(x(t), t)$:

$$\frac{dM(t)}{dt} + G_{xx} + M(t) G_{xp} + G_{xp}^T M(t) + M(t) G_{pp} M(t) = 0, \tag{12}$$

which is appended with an initial condition $M|_{t=0} = M_0 = \imath \epsilon I$, where ϵ is a positive number of order $O(1)$.

Although the Riccati equation (12) does not admit a global smooth solution in general, it turns out that complexifying the equation by specifying a complex initial value will guarantee that a global smooth solution exists because of the underlying symplectic structure associated with the related Hamiltonian system; see [18, 12, 21] for theoretical justification.

Now with the Hessian of the phase function at our disposal, we may solve the transport equation (5) for the amplitude $A(t) = A(x(t), t)$ along the ray path γ. Since $\tau_t(x(t), t) = -G(x(t), p(t))$ along the ray path, the transport equation (5) is reduced to the following:

$$\frac{dA}{dt} + \frac{A(x(t), t)}{2G} \left(V^2(x(t)) \text{trace}(M(t)) - G_x \cdot G_p - G_p^T M(t) G_p \right) = 0, \tag{13}$$

which is appended with a suitable initial condition $A|_{t=0} = A_0$.

At this stage, we are ready to construct a single Gaussian beam along the ray path γ by defining the following two global, smooth approximate functions for the phase and amplitude:

$$\tau(x,t) \equiv p(t) \cdot (x - x(t)) + \frac{1}{2}(x - x(t))^T M(t)(x - x(t)), \tag{14}$$

$$A(x,t) \equiv A(x(t),t) = A(t), \tag{15}$$

which are accurate near the ray path $\gamma = \{(x(t),t) : t \geq 0\}$. These two functions allow us to construct a single-beam asymptotic solution

$$\Phi(x,t) = A(x,t)\exp(\iota\omega\tau(x,t)). \tag{16}$$

This beam solution is concentrated on a single smooth curve $\gamma = \{(x(t),t) : t \geq 0\}$, which is the x-projection of the bicharacteristic $\{(x(t),p(t)) : t \geq 0\}$ emanating from (x_0,p_0) at $t = 0$. Because the phase $\tau(x,t)$ has an imaginary part, $\text{Im}(\tau(x,t)) = \frac{1}{2}(x - x(t))^T\text{Im}(M(t))(x - x(t))$, $\Phi(x,t)$ has a Gaussian profile of the form

$$\exp\left(-\frac{\omega}{2}(x - x(t))^T\text{Im}(M(t))(x - x(t))\right),$$

which is concentrated on the smooth ray path γ.

2.2 Incident and reflected beams for the wave equation

So far we have discussed how to apply Gaussian beam methods to the initial value problem of the wave equation, but the domain we are interested in is bounded. The boundary of the domain requires us to construct a reflected beam when an incident beam hits the boundary. The derivation here relies on results in [18].

Before continuing our discussion, we have to assume the non-grazing hypothesis:

$$\dot{x}_s(t_0) \cdot \nu(x(t_0)) > 0, \tag{17}$$

where $\dot{x}_s(t_0)$ denotes the direction of the incident ray, t_0 is the time when the incident ray hits the boundary ∂D at location $x(t_0)$, and ν denotes the outward normal vector to ∂D. In other words, the ray will not propagate along the boundary.

We further denote the incident and reflected beams by:

$$u_s = A_s(x,t)e^{\iota\omega\tau_s(x,t)}, \tag{18}$$

$$u_r = A_r(x,t)e^{\iota\omega\tau_r(x,t)}. \tag{19}$$

In order to satisfy the homogeneous Dirichlet boundary condition, we require that

$$(u_s + u_r)|_{(x(t_0),t_0)} = 0. \tag{20}$$

Substituting equations (18) and (19) into equation (20) yields:

$$A_s(x,t_0)e^{\iota\omega\tau_s(x,t_0)} = -A_r(x,t_0)e^{\iota\omega\tau_r(x,t_0)}. \tag{21}$$

Independence of ω demands that

$$\tau_s(x,t_0) = \tau_r(x,t_0), \tag{22}$$

$$A_s(x,t_0) = -A_r(x,t_0). \tag{23}$$

From equation (22), we impose the condition that all of their tangential and time derivatives be continuous at $(x(t_0),t_0)$. Therefore, differentiating with respect to t on both sides of equation (22) and using the eikonal equation (7) give us:

$$V(x(t_0))|p_s(x(t_0),t_0)| = V(x(t_0))|p_r(x(t_0),t_0)|. \tag{24}$$

In order to make the reflected beam incoming, we need $p_r \neq p_s$. Hence we have

$$p_r = (I - 2\nu\nu^T)p_s, \tag{25}$$

where ν is the outward normal at the reflection point.

For example, in 1-D cases the above condition (25) implies that

$$p_r = -p_s. \tag{26}$$

In 2-D cases, assuming that α is the angle between the tangential line of the boundary and the positive x_2-axis with $x = (x_1, x_2)$, we have

$$\begin{pmatrix} p_{1,r} \\ p_{2,r} \end{pmatrix} = \begin{pmatrix} \sin^2\alpha - \cos^2\alpha & -2\sin\alpha\cos\alpha \\ -2\sin\alpha\cos\alpha & \cos^2\alpha - \sin^2\alpha \end{pmatrix} \cdot \begin{pmatrix} p_{1,s} \\ p_{2,s} \end{pmatrix}, \tag{27}$$

where the outward normal at the reflection point is defined to be $(\cos\beta, \sin\beta)$ with $\beta = \pi - \alpha$.

The second-order derivatives of the phase function for the reflected beam can be determined by differentiating twice with respect to t in equation (22) and combining equations (10) and (11), and it follows that

$$G_p(x(t_0), p_s) \cdot G_x(x(t_0), p_s) + G_p^T(x(t_0), p_s)M_sG_p(x(t_0), p_s)$$
$$= G_p(x(t_0), p_r) \cdot G_x(x(t_0), p_r) + G_p^T(x(t_0), p_r)M_rG_p(x(t_0), p_r). \tag{28}$$

Substituting all the related quantities into equation (28) and using the continuity of the tangential components of the second-order derivatives of $\tau(x, t)$, we can determine the relation between the Hessian matrix M_s of the incident beam and the Hessian M_r of the reflected beam.

For example, we give those relations in three cases:

- 1-D *interval*:
$$M_r = M_s + 2p_s\frac{V_x}{V}. \tag{29}$$

- 2-D *rectangular domain*: let $x = (x_1, x_2)$. Assume that two sides of the rectangle are parallel to the x_1-axis and the other two sides are parallel to the x_2-axis:

  - If the beam hits the boundary parallel to the x_1-axis, then
  $$\begin{pmatrix} M_{11,r}, & M_{12,r} \\ M_{21,r}, & M_{22,r} \end{pmatrix} = \begin{pmatrix} M_{11,s} + 2\frac{p_{1,s}^2 + p_{2,s}^2}{p_{1,s}}\frac{V_{x_1}}{V}, & -M_{12,s} \\ -M_{21,s}, & M_{22,s} \end{pmatrix}. \tag{30}$$

  - If the beam hits the boundary parallel to the x_2-axis, then
  $$\begin{pmatrix} M_{11,r}, & M_{12,r} \\ M_{21,r}, & M_{22,r} \end{pmatrix} = \begin{pmatrix} M_{11,s}, & -M_{12,s} \\ -M_{21,s}, & M_{22,s} + 2\frac{p_{1,s}^2 + p_{2,s}^2}{p_{2,s}}\frac{V_{x_2}}{V} \end{pmatrix}. \tag{31}$$

  Here we simply ignore the situation when a beam hits a corner of the rectangle, since it causes diffraction and formula (20) does not apply any more. Since the Gaussian method is asymptotic, the numerical accuracy will not be degraded without those beams as those diffractions have exponentially small effects.

- 2-D *circular domain*: consider a unit disk with the boundary parameterized by angle θ. We have
$$\begin{pmatrix} M_{11,r} \\ M_{12,r} \\ M_{22,r} \end{pmatrix} = K_r^{-1} \cdot K_s \cdot \begin{pmatrix} M_{11,s} \\ M_{12,s} \\ M_{22,s} \end{pmatrix} + K_r^{-1} \cdot B, \tag{32}$$

where

$$K_r = \begin{pmatrix} \sin^2\theta & -2\sin\theta\cos\theta & \cos^2\theta \\ p_{1,r}\sin\theta & p_{2,r}\sin\theta - p_{1,r}\cos\theta & -p_{2,r}\cos\theta \\ p_{1,r}^2 & 2p_{1,r}p_{2,r} & p_{2,r}^2 \end{pmatrix}, \qquad (33)$$

$$K_s = \begin{pmatrix} \sin^2\theta & -2\sin\theta\cos\theta & \cos^2\theta \\ p_{1,s}\sin\theta & p_{2,s}\sin\theta - p_{1,s}\cos\theta & -p_{2,s}\cos\theta \\ p_{1,s}^2 & 2p_{1,s}p_{2,s} & p_{2,s}^2 \end{pmatrix}, \qquad (34)$$

$$B = \begin{pmatrix} (p_{1,r}-p_{1,s})\cos\theta + (p_{2,r}-p_{2,s})\sin\theta \\ 0 \\ (p_{1,s}^2 + p_{2,s}^2)\cdot(\frac{V_{x_1}}{V}(p_{1,s}-p_{1,r}) + \frac{V_{x_2}}{V}(p_{2,s}-p_{2,r})) \end{pmatrix}, \qquad (35)$$

where $p_{1,s}$, $p_{2,s}$, $p_{1,r}$ and $p_{2,r}$ are defined in (27). By symmetry, $M_{21,r} = M_{12,r}$, so all the entries of the Hessian matrix M_r are determined.

From equations (29)-(32), one can prove that the imaginary part from M_s to M_r is still symmetric positive definite [18, 3]. We thus have all the initial components for the reflected beams. The propagation of theses reflected beams follows the same equations in Section 2.1.

3   Fast Multiscale Gaussian beams

In order to construct a solution for the wave equation, it is also necessary for the asymptotic solution to satisfy the initial condition. However, since the initial condition may not have the form of a Gaussian wavepacket, we have to decompose the general initial profile into a superposition of Gaussian wavepackets. Here we apply fast multiscale Gaussian wavepacket transforms to initialize the beam propagation for the wave equation, resulting in fast multiscale Gaussian beams for wave equations in bounded domains.

3.1   Basic setup

We follow [17] closely. Let N be a sufficiently large positive integer in the sense that $[-N/2, N/2]^d$ is enough to cover the spectra of the initial conditions $f_1 \in H^1(D)$ and $f_2 \in L^2(D)$ in the Fourier domain. For simplicity, we assume that the domain is $D = [0,1]^d$. Without loss of generality, N is assumed to be the power of 2. We only consider the discrete version of the transform here. Define the spatial grid and Fourier grid to be

$$X = \{x = \left(\frac{n_1}{N}, \frac{n_2}{N}, \cdots, \frac{n_d}{N}\right) : 0 \leq n_1, n_2, \cdots, n_d < N, n_1, n_2, \cdots, n_d \in \mathbb{Z}\},$$

$$\Omega = \{\xi = (\xi_1, \xi_2, \cdots, \xi_d) : -\frac{N}{2} \leq \xi_1, \xi_2, \cdots, \xi_d < \frac{N}{2}, \xi_1, \xi_2, \cdots, \xi_d \in \mathbb{Z}\}.$$

Partition the Fourier domain Ω into Cartesian coronae C_l for $l \geq 1$ as follows:

$$C_1 = [-4, 4]^d,$$
$$C_l = \{\xi = (\xi_1, \xi_2, \cdots, \xi_d) : \max_{1 \leq s \leq d} |\xi_s| \in [4^{l-1}, 4^l]\}, \quad l \geq 2.$$

Each corona C_l is further partitioned into boxes:

$$B_{l,i} = \prod_{s=1}^{d} [2^l \cdot i_s, 2^l \cdot (i_s + 1)],$$

where $i = (i_1, i_2, \cdots, i_d)$ ranges over all possible choices which satisfy $B_{l,i} \subset C_l$. To each box $B_{l,i}$, we associate a smooth and compactly supported function $g_{l,i}$ with size $L_l = 2W^l$,

7

where $W^l = 2^l$ is the length of box $B_{l,i}$. The window function is approximately defined as

$$g_{l,i}(\xi) \approx e^{-\left(\frac{|\xi - \xi_{l,i}|}{\sigma_l}\right)^2}, \quad \xi \in \Omega, \tag{36}$$

where $\sigma_l = W^l/2$, and $\xi_{l,i}$ is the center of box $B_{l,i}$. Based on $g_{l,i}(\xi)$, we can define the conjugate filter $h_{l,i}(\xi)$ for each $B_{l,i}$:

$$h_{l,i}(\xi) = \frac{g_{l,i}(\xi)}{\sum_{l,i} g_{l,i}^2(\xi)}, \quad \xi \in \Omega. \tag{37}$$

It follows that the products of $g_{l,i}(\xi)$ and $h_{l,i}(\xi)$ form a partition of unity:

$$\sum_{l,i} g_{l,i}(\xi) h_{l,i}(\xi) = 1.$$

We now define two sets of functions $\varphi_{l,i,k}(x)$ and $\psi_{l,i,k}(x)$, which are both Gaussian wavepackets. Their constructions are based on $g_{l,i}(\xi)$ and $h_{l,i}(\xi)$, respectively.

In the Fourier domain, they are defined by:

$$\hat{\varphi}_{l,i,k}(\xi) = \frac{1}{L_l^{d/2}} e^{-2\pi i \frac{k \cdot \xi}{L_l}} g_{l,i}(\xi), \quad k \in \{0, 1, \cdots, L_l - 1\}, \tag{38}$$

$$\hat{\psi}_{l,i,k}(\xi) = \frac{1}{L_l^{d/2}} e^{-2\pi i \frac{k \cdot \xi}{L_l}} h_{l,i}(\xi), \quad k \in \{0, 1, \cdots, L_l - 1\}. \tag{39}$$

In the spatial domain, they can be numerically evaluated by:

$$\varphi_{l,i,k}(x) = \frac{1}{(NL_l)^{d/2}} \sum_{\xi \in \Omega} e^{2\pi i (x - \frac{k}{L_l})\xi} g_{l,i}(\xi), \quad k \in \{0, 1, \cdots, L_l - 1\}, \tag{40}$$

$$\psi_{l,i,k}(x) = \frac{1}{(NL_l)^{d/2}} \sum_{\xi \in \Omega} e^{2\pi i (x - \frac{k}{L_l})\xi} h_{l,i}(\xi), \quad k \in \{0, 1, \cdots, L_l - 1\}. \tag{41}$$

Here the subtraction in the spatial domain is understood modulus the periodic domain $[0, 1]^d$.

The forward multiscale Gaussian wavepacket transform for a given discretized function f on X is defined by:

$$c_{l,i,k} = <\psi_{l,i,k}, f> = <\hat{\psi}_{l,i,k}, \hat{f}> = \sum_{\xi \in \Omega} \frac{1}{L_l^{d/2}} e^{-2\pi i \frac{k \cdot \xi}{L_l}} h_{l,i}(\xi) \hat{f}(\xi), \tag{42}$$

where $\hat{f}(\xi)$ is the discretized Fourier transform of f, and $< \cdot, \cdot >$ denotes the L^2 inner product. It is proved that $f \in L^2(D)$ can be expressed as [17]:

$$f(x) = \sum_{l,i,k} c_{l,i,k} \varphi_{l,i,k}(x). \tag{43}$$

By the definition (40) of $\varphi_{l,i,k}(x)$, it approximately equals,

$$\varphi_{l,i,k} \approx \left(\sqrt{\frac{\pi}{NL_l}} \sigma_l\right)^d e^{2\pi i (x - \frac{k}{L_l})\xi_{l,i}} e^{-\sigma_l^2 \pi^2 |x - \frac{k}{L_l}|^2}, \quad x \in X, \tag{44}$$

which can be taken as a Gaussian wavepacket centered at $\frac{k}{L_l}$ with frequency $\xi_{l,i}$. Together with equation (43), this allows us to decompose a general $L^2(D)$ function into a superposition of Gaussian wavepackets. The resulting fast multiscale Gaussian wavepacket transforms have the complexity $O(N^d \log N)$; see [17].

3.2 Initialization and propagation for the wave equation

We first assume that D is a Cartesian domain in $\mathbb{R}^d$. With all the preparation above, we are now ready to employ multiscale Gaussian wavepacket transforms to decompose functions $f_1 \in H^1(D)$ and $f_2 \in L^2(D)$ into Gaussian wavepackets. Following [17], we decompose the initial data by the forward transform (42):

$$f_1(x) = \sum_{l,i,k} a_{l,i,k} \varphi_{l,i,k}(x), \tag{45}$$

$$f_2(x) = \sum_{l,i,k} b_{l,i,k} \varphi_{l,i,k}(x). \tag{46}$$

Assume that the global asymptotic solution for equation (1) has the form:

$$u_{GB}(x,t) = \sum_{l,i,k} (c^+_{l,i,k} \Phi^+_{l,i,k}(x,t) + c^-_{l,i,k} \Phi^-_{l,i,k}(x,t)), \tag{47}$$

where "+" and "−" represent two different wave modes. If we suppress the superscripts "$\pm$", $\Phi_{l,i,k}(x,t)$ is a Gaussian beam propagating in the space-time domain with the initial condition $\varphi_{l,i,k}(x)$. It can be obtained by solving the following equations:

$$\begin{aligned}
\dot{x} &= G_p, \\
\dot{p} &= -G_x, \\
\dot{M} &= -(G_{xp})^T M - M G_{xp} - M G_{pp} M - G_{xx}, \\
\dot{A} &= -\frac{A}{2G} \left(V^2(x)\text{trace}(M) - G_x \cdot G_p - G_p^T M G_p \right)
\end{aligned} \tag{48}$$

with the initial conditions:

$$\begin{aligned}
x|_{t=0} &= \frac{k}{L_l}, \\
p|_{t=0} &= 2\pi \frac{\xi_{l,i}}{|\xi_{l,i}|}, \\
M|_{t=0} &= i \cdot 2\pi^2 \frac{\sigma_l^2}{|\xi_{l,i}|} I, \\
A|_{t=0} &= \left(\sqrt{\frac{\pi}{NL_l}} \sigma_l \right)^d,
\end{aligned} \tag{49}$$

where I means the identity matrix. According to Section 2.2, at a reflection point we have to set:

$$\begin{aligned}
x_r|_{t=t_0} &= x_s|_{t=t_0}, \\
p_r|_{t=t_0} &= r_1(p_s), \\
M_r|_{t=t_0} &= r_2(M_s), \\
A_r|_{t=t_0} &= -A_s|_{t=t_0}.
\end{aligned} \tag{50}$$

Expressions of $r_1(\cdot)$ and $r_2(\cdot)$ depend on the geometry of the domain. In particular, the explicit form of $r_1(p_s)$ is given in (26) and (27), and the explicit form of $r_2(M_s)$ is given in (29), (30), and (32) for three special cases.

The Gaussian Beam solution corresponding to $\varphi_{l,i,k}(x)$ is given by

$$\Phi_{l,i,k}(x,t) = A_{l,i,k}(x,t) e^{i \cdot |\xi_{l,i}| \tau_{l,i,k}(x,t)} \tag{51}$$

9

with

$$\tau_{l,i,k}(x,t) \equiv p_{l,i,k}(t)(x - x_{l,i,k}(t)) + \frac{1}{2}(x - x_{l,i,k}(t))^T M_{l,i,k}(x - x_{l,i,k}(t)),$$

$$A_{l,i,k}(x,t) \equiv A_{l,i,k}(x(t),t) = A_{l,i,k}(t).$$

Now we only have to determine the coefficients $c_{l,i,k}^{\pm}$ to complete the construction. Letting $t = 0$ in equation (47) and using equation (45) yield

$$c_{l,i,k}^{+} \varphi_{l,i,k}(x,t) + c_{l,i,k}^{-} \varphi_{l,i,k}(x,t) = a_{l,i,k} \varphi_{l,i,k}(x). \tag{52}$$

Differentiate (47) with respect to t on both sides, use equation (13) and let $t \to 0$:

$$(c_{l,i,k}^{+} - c_{l,i,k}^{-})\left(\frac{D_0}{2G^{+}(x(0),p(0))} + \imath \cdot |\xi_{l,i}| G^{+}(x,p(0)) \right) \varphi_{l,i,k}(x) = u_t|_{t=0} = b_{l,i,k} \varphi_{l,i,k}(x), \tag{53}$$

where

$$D_0 = V^2 M(0) - G_p^{+}(x(0),p(0))(G_x^{+}(x(0),p(0)) + M(0)G_p^{+}(x(0),p(0))).$$

Since $|\xi_{l,i}|$ captures the frequency information of f_1 and f_2, $|\xi_{l,i}|$ is large in comparison to D_0. In this sense, D_0 is negligible and $G(x,p(0))$ can also be approximated by $G(x(0),p(0))$ due to the narrow support of $\varphi_{l,i,k}(x)$. Therefore, it is reasonable to have from (53)

$$(c_{l,i,k}^{+} - c_{l,i,k}^{-})\left(\imath \cdot |\xi_{l,i}| G^{+}(x,p(0)) \right) \varphi_{l,i,k}(x) \approx u_t|_{t=0} = b_{l,i,k} \varphi_{l,i,k}(x). \tag{54}$$

Solving equations (52) and (54) for $c_{l,i,k}^{+}$ and $c_{l,i,k}^{-}$, we get

$$c_{l,i,k}^{+} = \frac{1}{2}\left(a_{l,i,k} - \frac{b_{l,i,k}}{\imath \cdot G^{+}(\frac{k}{L_l}, 2\pi \xi_{l,i})} \right), \tag{55}$$

$$c_{l,i,k}^{-} = \frac{1}{2}\left(a_{l,i,k} + \frac{b_{l,i,k}}{\imath \cdot G^{+}(\frac{k}{L_l}, 2\pi \xi_{l,i})} \right). \tag{56}$$

Once all the coefficients $c_{l,i,k}^{\pm}$ and the related quantities $x_{l,i,k}^{\pm}(t)$, $p_{l,i,k}^{\pm}(t)$, $M_{l,i,k}^{\pm}(t)$, and $A_{l,i,k}^{\pm}(t)$ are available, the global asymptotic solution can thus be determined by formula (47).

4 Numerical strategies for treating bounded domains

4.1 Decomposition of initial data

Since the fast multiscale Gaussian wavepacket transform is designed for periodic functions, the initial data f_1 and f_2 originally defined in a bounded convex domain D need to be periodically extended to a rectangular domain. However, since the homogeneous Dirichlet datum is specified on the boundary of D, such a continuation should allow the resulting solution for the wave equation to satisfy the boundary condition naturally. To illustrate this, we consider three situations.

Rectangular domains. First we consider one-dimensional case. Let $D=[0,L]$, and let the initial data be compactly supported away from the boundary and satisfy the following conditions:

$$f_i(0) = f_i'(0) = 0, \quad f_i(L) = f_i'(L) = 0, \quad i = 1, 2.$$

These two functions are continued as odd periodic functions of period $2L$:

$$f_i(x) = -f_i(-x), \quad \text{for } -L \le x \le 0; \quad f_i(x + 2L) = f_i(x), \quad i = 1, 2. \tag{57}$$

If the velocity function $V(x)$ is constant, then when restricted to the original domain D the d'Alembert formula for the pure initial-value problem of the 1-D wave equation with the periodic data (57) actually yields a solution satisfying the homogeneous Dirichlet data for the initial-boundary value problem defined in D. This motivates us to first carry out odd periodic continuation for the initial data and then apply the fast multiscale Gaussian wavepacket transform to decompose the continued data into Gaussian wavepackets. To recover the initial data (and the beam solution) in the original domain, we will only use the corresponding wavepackets with centers in the domain D and utilize the summation process as described in Subsection 4.2.

Such an odd, periodic continuation process apparently can be applied to compactly supported initial data specified in two- and three-dimensional rectangular domains, and the resulting odd periodic functions are compatible with the homogeneous Dirichlet data as well.

Two-dimensional circular domains. Let D be a disk centered at O with radius r, and let the initial data be compactly supported in D away from the boundary. We embed D into a rectangular domain $[0, L] \times [0, L]$ so that $L \geq 4r$ and the center O is located at the center of the rectangular domain. To continue the initial data across the disk to the rectangular domain so as to be compatible with the homogeneous Dirichlet data on the circle ∂D, we will first carry out odd continuation of the initial data in the sense of geometric inversion (generalization of reflection) with respect to the circle ∂D. As shown in Figure 1, given a point $P \in [0, L]^2 \setminus D$, we may find a point Q on the line OP such that $|OQ||OP| = r^2$, where $|OQ|$ is the Euclidean distance between O and Q, and the so-defined Q is called the inverse of P with respect to the circle ∂D; according to the inverse Q of the point P, we continue the initial data across ∂D by defining

$$f_i(P) = -f_i(Q), \quad i = 1, 2. \tag{58}$$

By this odd continuation, the original initial data are continued to the rectangular domain $[0, L]^2$. Since the fast Gaussian wavepacket transforms consist of localized functions which are exponentially small away from the centers, the initial datum far away from D has an exponentially small effect on the initial datum inside D in terms of recovering the initial data inside D from the Gaussian wave packet decomposition; therefore, it is reasonable to ignore the continued initial data beyond the domain $[0, L]^2$ and periodize these initial data to be of period L along each coordinate direction. Consequently, we may apply the fast multiscale Gaussian wavepacket transform to decompose the continued initial data on $[0, L]^2$ and recover the initial data with wavepackets centered in D by the summation method discussed in Subsection 4.2.
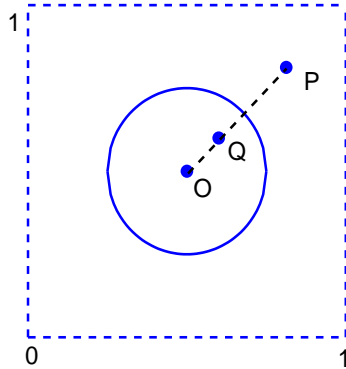

Figure 1: *Odd periodic continuation for a circular domain*

Two-dimensional bounded strictly convex domains. We may extend the above idea of odd periodic continuation to initial data defined in arbitrary bounded strictly convex domains. Let D be a bounded strictly convex domain and let P be a point outside of the closure of D. Due to the strict convexity of D, there exists a unique projection $T \in \partial D$ of the point P so that the line defined by T and P is orthogonal in the Euclidean inner product to the tangent plane at $T \in \partial D$. Since ∂D is a strict convex curve, the curvature at each point along the boundary is positive so that the osculating circle at the boundary point T is well defined, is tangent to the tangent plane at T, and is located on the same side of the tangent plane as the convex domain. By the separation theorem for convex sets, P is outside of the osculating circle at T. These observations imply that we may adopt the principle of geometric inversion in a pointwise sense with respect to the osculating circle to continue the compactly supported initial data across the convex domain. This idea is explored in an ongoing project, and we will report on this in another paper.

4.2   Beam summation

By design, each individual Gaussian beam satisfies the wave equation asymptotically, and the initial data are satisfied by suitable linear combinations of many beams. The question now is how to enforce the homogeneous Dirichlet boundary condition for each individual beam. By construction, each beam is reflected at the boundary according to the geometrical-optics ray theory, by which the homogeneous Dirichlet datum is satisfied on the central ray of each beam; however, since the off-central parts of each beam also contribute to the overall solution, we need to make sure that the off-central parts satisfy the homogeneous Dirichlet boundary condition as well. To see this point more clearly, we illustrate this phenomenon in the one-dimensional case as in Figure 2, where a part of the beam solution ("tail") goes beyond outside the domain so that the homogeneous Dirichlet boundary condition is violated. Therefore, we need to address such situations.
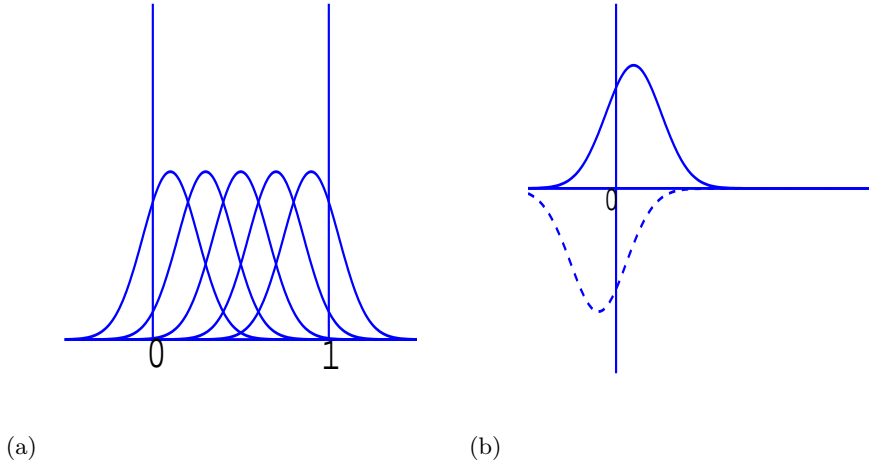

(a)   (b)

Figure 2: *(a)Tail exceeds the boundary; (b)Image principle*

Rectangular domains. Motivated by the method of images, the remedy here is to imagine the boundary as a mirror and the tail of the beam is reflected back from the boundary. Intuitively, the beam can "see" itself through the boundary with an opposite sign and the field inside the domain is the superposition of these two kinds of beams; see Figure 2(b). This is called the "image principle", and it is analogous to defining geometrical-optics ingredients for constructing incident and reflected beams in Section 2.2 so that the

homogeneous Dirichlet boundary condition is satisfied. Similar to the method of images, the beam summation in this way is exact for the wave equation with a constant velocity. Due to the high frequency, the effective area of a beam is small compared to the whole domain, and the velocity is almost constant in such a small area, so the algorithm still works even for a variable velocity.

Circular domains. In this case, if the effective area of any beam gets out of the computational domain, we need to reflect it back across the circular boundary, since the homogeneous Dirichlet boundary condition on the circle has to be satisfied. The way to do the reflection is similar to the procedure in the initialization process in a circular domain, but is done reversely. Namely, we find the area inside the computational domain D, denoted by S^*, that is "inverse" to the effective area outside D, denoted by S. For any point in S^*, the beam value at that point should be modified by adding an opposite value from its inverse point in S.

Two-dimensional bounded strictly convex domains. For a general convex domain with a curved boundary, we apply the idea of geometrical inversion as we do in the initialization. More specifically, for a beam centered at P in the interior of domain D with its effective area outside the domain, a unique point T on the boundary ∂D can be found such that PT is orthogonal to the tangent plane at T provided P is very close to ∂D. The assumption is reasonable as the support of Gaussian beam is very small. Now the inversion point of P is found through the osculating circle at T. As we have done in the circular domain, for any point affected by the beam centered at P, the value at that point should be modified by adding a value from the inversion point of P. The implementation of this idea is ongoing.

4.3 Identifying significant beams

To develop an efficient Gaussian beam method, it is critical to control the number of launched beams. Ideally, one would like to achieve the asymptotic accuracy by launching the least number of beams. A common wisdom is to identify significant beams according to the amplitude function; however, the following example shows that the amplitude function alone may not be a good indicator for choosing significant beams.

Consider the one-dimensional wave equation posed in $D = [0, 1]$ with the velocity function $V(x) = 1 + bx$, where the constant b is chosen such that $V(x)$ is positive on $D = [0, 1]$. By the Lipschitz continuity of the Hamiltonian flow $\{(x(t), p(t)) : 0 \leq t \leq T\}$, the function $p(t)$ has the same sign as its initial value p_0 in a finite time period. Assuming that $G(x, p) = V(x)|p|$ and $p_0 > 0$, we obtain that

$$
\begin{aligned}
\frac{dp}{dt} &= -bp, \quad p|_{t=0} = p_0, \\
\frac{dM}{dt} &= -2bM, \quad M|_{t=0} = M_0, \\
\frac{dA}{dt} &= \frac{1}{2}bA, \quad A|_{t=0} = A_0.
\end{aligned}
$$

It follows that

$$
\begin{aligned}
p(t) &= p_0\, e^{-bt}, \\
M(t) &= M_0\, e^{-2bt}, \\
A(t) &= A_0\, e^{\frac{bt}{2}}.
\end{aligned}
$$

Consequently, if $b \neq 0$, the amplitude function can be either growing or decaying exponentially, depending on the sign of b. On the other hand, as analyzed in [16, 17], the beam width is controlled by the Hessian $M(t)$. As the above solutions indicate that $M(t)$ and $A(t)$ tend to change in the opposite directions, we need to combine these two quantities into one to identify significant beams, which is achieved by the following theorem.

13

For a beam $\Phi(x,t)$ given in the form of (51) without subscript, consider the following quantity:

$$E(\Phi(x,t)) = \frac{C_\Phi |A(x,t)|^2}{\sqrt{det(\Im(M(t)))}}$$

which combines the amplitude and the beam width; here C_Φ is some scaling constant related to the weight of the current beam. It can be shown that $E(\Phi(x,t))$ does not change too much in the propagation in the sense of the following theorem.

Theorem 4.1 *Assume that $V(x)$ is $C^2(D)$. There exist positive constants C_1 and C_2, only depending on $V(x)$, such that $E(\Phi(x,t))$ satisfies*

$$C_1 \leq \frac{E(\Phi(x,t))}{E(\Phi(x,0))} \leq C_2$$

for $0 \leq t \leq T$.

Proof By using the definition of $G(x,p)$, the transport equation can be rewritten as:

$$\begin{aligned}
\frac{d\ln A}{dt} &= -(2G)^{-1}(V^2(x(t))\text{trace}(M(t)) - G_x \cdot G_p - G_p^T M(t) G_p) \\
&= -\frac{1}{2}\text{trace}(G_{pp}M(t) + G_{xp}) + G^{-1}G_x \cdot G_p \\
&= -\frac{1}{2}\text{trace}(G_{pp}M(t) + G_{xp}) + \frac{d\ln V(x(t))}{dt}.
\end{aligned} \quad (59)$$

The last step is obtained by using

$$\frac{d\ln V(x(t))}{dt} = \frac{V_x}{V} \cdot \dot{x} = V_x \cdot \frac{p}{|p|} = G^{-1}G_x \cdot G_p.$$

Thus, we have:

$$|A(t)|^2 = \frac{|A(0)|^2 |V(x(t))|^2}{|V(x(0))|^2} \exp\left(-\int_0^t \text{trace}(G_{pp}\Re(M(s)) + G_{xp})ds\right). \quad (60)$$

The differential equation for $det(\Im(M(t)))$ is:

$$\begin{aligned}
\frac{d\ln\det(\Im(M(t)))}{dt} &= \text{trace}\left(\frac{d\Im(M(t))}{dt}(\Im(M(t)))^{-1}\right) \\
&= -\text{trace}\left(G_{xp} + \Re(M(t))G_{pp} + \Im(M(t))\left(G_{xp}^T + G_{pp}\Re(M(t))\right)(\Im(M(t)))^{-1}\right) \\
&= -2\text{trace}\left(G_{xp} + \Re(M(t))G_{pp}\right). \quad (61)
\end{aligned}$$

The last equality is given by the trace invariance under similarity transformation. Hence:

$$det(\Im(M(t))) = det(\Im(M(0)))exp\left(-2\int_0^t \text{trace}(G_{pp}\Re(M(s)) + G_{xp})ds\right). \quad (62)$$

Combining (60) and (62) yields the proof. ∎

Based on Theorem 4.1, $E(\Phi(x,t))$ is bounded during the propagation of a beam, even at reflections, since both $|A(t)|$ and $\Im(M(t))$ are unchanged at a reflection point. In particular, $E(\Phi_{l,i,k}(x,0)) = C(d)c_{l,i,k}|\xi_{l,i}|^{d/2}$, where $C(d)$ only depends on the dimension d and N. We thus use $E(\Phi(x,t))$ as the criteria to choose the significant beams, which is better than using amplitude only.

4.4 Overall algorithm

Here is a sketch for the overall algorithm for the initial boundary value problem (1) by the multiscale Gaussian beam method:

- Decompose the initial condition into a summation of wavepackets by the multiscale Gaussian wavepacket transform (42) and determine the coefficients $c_{l,i,k}^+$ and $c_{l,i,k}^-$ by equations (55) and (56).

- Choose $\epsilon > 0$, and evaluate $E(\Phi_{l,i,k}(x,0))$. If $E(\Phi_{l,i,k}(x,0)) > \epsilon$, propagate the beam by solving the system (48) with the initial condition (49) and the reflection condition (50); otherwise the beam is dropped.

- At the time T, sum up all the beams by the image principle given in Section 4.2.

We now analyze the computational complexity of the overall algorithm, which consists of three parts. The first part is the initialization by multiscale Gaussian wavepacket transform, which has a complexity $O(N^d \log N)$. The second part is the propagation of all the Gaussian beams. The computation for tracing a single beam over a finite time period can be accomplished in $O(1)$ steps, so the total cost for this part is proportional to the total number of beams. For most of the applications, like point sources, plane waves, and curvilinear wavefronts, the number of beams is supposed to be small at given accuracy ϵ. The final part is the summation step. As the support of each Gaussian beam is of size $O(N^{1/2})$ in each dimension, each beam at time T covers about $O(N^{d/2})$ points. Overall, the computational complexity is $O(N^d \log N + C \cdot N^{d/2})$, where C denotes the number of beams being traced. It is much more efficient compared to the $O(N^{d+1})$ cost of standard finite difference or finite element methods.

5 Convergence results

The convergence result of Gaussian beam methods for pure initial-value problems of wave equations was discussed in many papers; see [13, 22, 2]. In terms of wave equations in bounded convex domains, the convergence result for single-scale Gaussian beam methods based on the FBI transform was provided by [3]. Inspired by the convergence results in [2] of multiscale Gaussian beam methods for pure initial-value problems of wave equations, we prove that the multiscale Gaussian beam method for wave equations in bounded convex domains is convergent.

The main convergence result is stated in the following theorem.

Theorem 5.1 *Assume that $u(x,t)$ is the exact solution of the wave equation (1) and $u_{GB}(x,t)$ is the solution based on the multiscale Gaussian beam method. T is a given finite number. The initial conditions satisfy:*

$$f_1(x) = \sum_{l,i,k} a_{l,i,k} \varphi_{l,i,k}(x), \tag{63}$$

$$f_2(x) = \sum_{l,i,k} b_{l,i,k} \varphi_{l,i,k}(x). \tag{64}$$

Let $\xi_{min} = \min_{l,i,k} \{|\xi_{l,i}|: |\xi_{l,i}|$ associated with $\varphi_{l,i,k}\} \geq 4$. We have

$$\sup_{t\in[0,T]} \|u(\cdot,t) - u_{GB}(\cdot,t)\|_{H^1(D)} + \sup_{t\in[0,T]} \|\partial_t u(\cdot,t) - \partial_t u_{GB}(\cdot,t)\|_{L^2(D)} \tag{65}$$

$$\preceq \frac{1}{\xi_{min}^{1/2}} (\|f_1\|_{H^1(D)} + \|f_2\|_{L^2(D)}). \tag{66}$$

Here "$\preceq$" denotes the upper bound up to a constant multiple C, which is independent of the frequency ξ_{min}. The assumption on the initial conditions (63) and (64) is based on

the fact that the error introduced by the Gaussian wavepacket transform is negligible [2]. Since we are concerned with high frequency waves, the lower bound on the frequency is also reasonable.

To prove the theorem, we recall some lemmas. By the construction of Gaussian beams, let $e(x,t) = u(x,t) - u_{GB}(x,t)$; it follows that $e(x,t)$ satisfies:

$$
\begin{cases}
e_{tt} - V^2(x)\Delta e(x,t) = Pu_{GB}(x,t), \\
\quad\quad e|_{t=0} = 0, \\
\quad\quad e_t|_{t=0} = 0, \\
\quad\quad e|_{x\in\partial D} = Bu_{GB}(x,t).
\end{cases}
\tag{67}
$$

The two terms $Pu_{GB}(x,t)$ and $Bu_{GB}(x,t)$ represent the propagation error and the boundary error caused by the approximation of the Gaussian beam method, respectively. By the classical PDE theory for the initial boundary value problems of wave equations, we have:

Lemma 5.2 *Assume that $u(x,t)$ is the exact solution of the wave equation* (1) *and $u_{GB}(x,t)$ is the solution based on the Gaussian beam method. Define $e(x,t) = u(x,t) - u_{GB}(x,t)$. Then the following estimate holds,*

$$
\sup_{t\in[0,T]} \|e(\cdot,t)\|_{H^1(D)} + \sup_{t\in[0,T]} \|\partial_t e(\cdot,t)\|_{L^2(D)}
$$
$$
\preceq \sup_{t\in[0,T]} \|Pu_{GB}\|_{L^2(D)} + \|Bu_{GB}\|_{H^1([0,T]\times\partial D)}.
$$

Assuming that the initial conditions are given in equations (63) and (64), Bao et al [2] essentially proved the following convergence of the propagation error:

Theorem 5.3 *([2])* $\sup_{t\in[0,T]} \|Pu_{GB}\|_{L^2(D)} \preceq \frac{1}{\xi_{min}^{1/2}}(\|f_1\|_{H^1(D)} + \|f_2\|_{L^2(D)})$.

Hence, we only need to prove:

$$
\|Bu_{GB}\|_{H^1([0,T]\times\partial D)} \preceq \frac{1}{\xi_{min}^{1/2}}(\|f_1\|_{H^1(D)} + \|f_2\|_{L^2(D)}).
\tag{68}
$$

Before we proceed to the proof, we need two important lemmas. The first one gives the relation between the coefficients and the norm of the initial conditions (45) and (46).

Lemma 5.4 *([17]) Let $\xi_{l,i}$, $a_{l,i,k}$, $b_{l,i,k}$, $c_{l,i,k}^+$, and $c_{l,i,k}^-$ be defined in* (44), (45), (46), (55), *and* (56), *respectively. Then*

$$
\sum_{l,i,k} \xi_{l,i}^2(|c_{l,i,k}^+|^2 + |c_{l,i,k}^-|^2) \preceq \sum_{l,i,k}(\xi_{l,i}^2|a_{l,i,k}|^2 + |b_{l,i,k}|^2) \preceq \|f_1\|_{H^1(D)} + \|f_2\|_{L^2(D)}.
\tag{69}
$$

The proof of this Lemma is based on the Fourier transform and the boundedness of the velocity $V(x)$; see [17]. In fact, these three quantities are equivalent under suitable assumptions. The second lemma is the following.

Lemma 5.5 *([2]) Assume that the phase function associated to any beam $\Phi_{l,i,k}(x,t)$ in equation* (51) *satisfies the condition that the imaginary part of the Hessian matrix $M_{l,i,k}$ is symmetric and positive definite. Let $d_{l,i,k}$ be complex numbers such that $\sum_{l,i,k}|d_{l,i,k}|^2 < \infty$, and $d_{l,i,k} = 0$ for small l. $H_{l,i,k}(x,t)$ is a differentiable function both in x and t. Assume that there exists an integer $n > 0$ such that for each (l,i,k) we have $H_{l,i,k}(x,t) = O(|x - x_{l,i,k}(t)|^n)$. Then*

$$
\|\sum_{l,i,k} \xi_{l,i}^{\frac{n}{2}} d_{l,i,k}\Phi_{l,i,k}(x,t) \cdot H_{l,i,k}(x,t)\|_{L^2(D)}^2 \preceq \sum_{l,i,k}|d_{l,i,k}|^2.
\tag{70}
$$

16

Its proof fully utilizes the exponential decay of Gaussian beams; details can be found in [2]. It shows that the interaction between different beams can be controlled. Now we are ready to prove the main result.

Proof of the main theorem. Let

$$u_{GB}(x,t) = u_{GB}^+(x,t) + u_{GB}^-(x,t),$$

where $u_{GB}^+(x,t) = \sum_{l,i,k} c_{l,i,k}^+ \Phi_{l,i,k}^+(x,t)$ and $u_{GB}^-(x,t) = \sum_{l,i,k} c_{l,i,k}^- \Phi_{l,i,k}^-(x,t)$.

We discuss $u_{GB}^+(x,t)$ only since $u_{GB}^-(x,t)$ can be treated in the same way, and for simplicity, we drop the superscript "+". Each propagating beam $\Phi_{l,i,k}(x,t)$ will bounce back and forth in the domain up to finite times N_0. Without loss of generality, we assume that each beam reflects N_0 times, since we can always add zero beams if it does not. Use $\Phi_{l,i,k}^p(x,t)$ to denote the pth ($0 \le p \le N_0$) reflection of the beam. It is easy to see that except $\Phi_{l,i,k}^0(x,t)$ and $\Phi_{l,i,k}^{N_0}(x,t)$, for any p, $\Phi_{l,i,k}^p(x,t)$ can be both an incident beam and a reflected beam and we add "s" and "r" to denote the difference. Now the boundary value can be rewritten as:

$$Bu_{GB}(x,t)|_{x\in\partial D} = \sum_{l,i,k} \sum_{p=0}^{N_0-1} (c_{l,i,k}\Phi_{l,i,k}^{p,s}(x,t) + c_{l,i,k}\Phi_{l,i,k}^{p+1,r}(x,t))|_{x\in\partial D}$$

$$= \sum_{l,i,k} \sum_{p=0}^{N_0-1} (c_{l,i,k}A_{l,i,k}^{p,s}(x,t)e^{i\cdot|\xi_{l,i}|\tau_{l,i,k}^{p,s}(x,t)} + c_{l,i,k}A_{l,i,k}^{p+1,r}(x,t)e^{i\cdot|\xi_{l,i}|\tau_{l,i,k}^{p+1,r}(x,t)}).$$

$$\tag{71}$$

Let $x_{l,i,k}^{p,s}$ and $t_{l,i,k}^{p,s}$ denote the position and time that the pth reflected beam hits the boundary. By construction of reflected beams in equations (22) and (23), for each (l,i,k) we have:

$$A_{l,i,k}^{p,s}(\overline{x},t)|_{\overline{x}\in\partial D} = A_{l,i,k}^{p,s}(x_{l,i,k}^{p,s},t_{l,i,k}^{p,s}) + O(\overline{x} - x_{l,i,k}^{p,s}, t - t_{l,i,k}^{p,s})$$

$$A_{l,i,k}^{p+1,r}(\overline{x},t)|_{\overline{x}\in\partial D} = A_{l,i,k}^{p+1,r}(x_{l,i,k}^{p,s},t_{l,i,k}^{p,s}) + O(\overline{x} - x_{l,i,k}^{p,s}, t - t_{l,i,k}^{p,s})$$

$$= -A_{l,i,k}^{p,s}(x_{l,i,k}^{p,s},t_{l,i,k}^{p,s}) + O(\overline{x} - x_{l,i,k}^{p,s}, t - t_{l,i,k}^{p,s}) \tag{72}$$

and

$$\tau_{l,i,k}^{p,s}(\overline{x},t)|_{\overline{x}\in\partial D} = \tau_{l,i,k}^{p,s}(x_{l,i,k}^{p,s},t_{l,i,k}^{p,s}) + (\partial_{\overline{x}}\tau_{l,i,k}^{p,s}, \partial_t\tau_{l,i,k}^{p,s}) \cdot (\overline{x} - x_{l,i,k}^{p,s}, t - t_{l,i,k}^{p,s})$$

$$+ (\overline{x} - x_{l,i,k}^{p,s}, t - t_{l,i,k}^{p,s}) \cdot \begin{pmatrix} \partial_{\overline{x}\overline{x}}\tau_{l,i,k}^{p,s}, & \partial_{\overline{x}t}\tau_{l,i,k}^{p,s} \\ (\partial_{\overline{x}t}\tau_{l,i,k}^{p,s})^T, & \partial_{tt}\tau_{l,i,k}^{p,s} \end{pmatrix} \cdot \begin{pmatrix} \overline{x} - x_{l,i,k}^{p,s} \\ t - t_{l,i,k}^{p,s} \end{pmatrix}$$

$$+ O\begin{pmatrix} \overline{x} - x_{l,i,k}^{p,s} \\ t - t_{l,i,k}^{p,s} \end{pmatrix}^3, \tag{73}$$

$$\tau_{l,i,k}^{p+1,r}(\overline{x},t)|_{\overline{x}\in\partial D} = \tau_{l,i,k}^{p+1,r}(x_{l,i,k}^{p,s},t_{l,i,k}^{p,s}) + (\partial_{\overline{x}}\tau_{l,i,k}^{p+1,r}, \partial_t\tau_{l,i,k}^{p+1,r}) \cdot (\overline{x} - x_{l,i,k}^{p,s}, t - t_{l,i,k}^{p,s})$$

$$+ (\overline{x} - x_{l,i,k}^{p,s}, t - t_{l,i,k}^{p,s}) \cdot \begin{pmatrix} \partial_{\overline{x}\overline{x}}\tau_{l,i,k}^{p+1,r}, & \partial_{\overline{x}t}\tau_{l,i,k}^{p+1,r} \\ (\partial_{\overline{x}t}\tau_{l,i,k}^{p+1,r})^T, & \partial_{tt}\tau_{l,i,k}^{p+1,r} \end{pmatrix} \cdot \begin{pmatrix} \overline{x} - x_{l,i,k}^{p,s} \\ t - t_{l,i,k}^{p,s} \end{pmatrix}$$

$$+ O\begin{pmatrix} \overline{x} - x_{l,i,k}^{p,s} \\ t - t_{l,i,k}^{p,s} \end{pmatrix}^3. \tag{74}$$

Here $\overline{x} \in \partial D$ and the notation $\partial_{\overline{x}}$ means the partial derivative with respect to the tangential component of the boundary. By the continuity of the tangential components of the phase function τ up to the second order, we get:

$$\tau_{l,i,k}^{p,s}(\overline{x},t)|_{\overline{x}\in\partial D} - \tau_{l,i,k}^{p+1,r}(\overline{x},t)|_{\overline{x}\in\partial D} = O\begin{pmatrix} \overline{x} - x_{l,i,k}^{p,s} \\ t - t_{l,i,k}^{p,s} \end{pmatrix}^3. \tag{75}$$

17

Now combining equations (72) and (75) yields:

$$
\begin{aligned}
&A_{l,i,k}^{p,s}(x,t)e^{\imath\cdot|\xi_{l,i}|\tau_{l,i,k}^{p,s}(x,t)} + A_{l,i,k}^{p+1,r}(x,t)e^{\imath\cdot|\xi_{l,i}|\tau_{l,i,k}^{p+1,r}(x,t)}|_{x\in\partial D}\\
=&(A_{l,i,k}^{p,s}(x,t) + A_{l,i,k}^{p+1,r}(x,t))e^{\imath\cdot|\xi_{l,i}|\tau_{l,i,k}^{p,s}(x,t)}|_{x\in\partial D}\\
&+ A_{l,i,k}^{p+1,r}(x,t)e^{\imath\cdot|\xi_{l,i}|\tau_{l,i,k}^{p,s}(x,t)}(e^{\imath\cdot|\xi_{l,i}|(\tau_{l,i,k}^{p+1,r}(x,t)-\tau_{l,i,k}^{p,s}(x,t))} - 1)|_{x\in\partial D}\\
=&e^{\imath\cdot|\xi_{l,i}|\tau_{l,i,k}^{p,s}(x,t)}\cdot O(x - x_{l,i,k}^{p,s}, t - t_{l,i,k}^{p,s})|_{x\in\partial D}\\
&+ A_{l,i,k}^{p+1,r}(x,t)e^{\imath|\xi_{l,i}|\tau_{l,i,k}^{p,s}(x,t)}|\xi_{l,i}|\cdot O(x - x_{l,i,k}^{p,s}, t - t_{l,i,k}^{p,s})^3|_{x\in\partial D}.
\end{aligned}
\tag{76}
$$

Recall the fact that with the non-grazing hypothesis (17) the Hessian of the beam on the boundary $[0,T]\times\partial D$ still has a symmetric positive definite imaginary part [18, 3], so instead of the space domain D, we can apply Lemma 5.5 to $Bu_{GB}(x,t)$ on $[0,T]\times\partial D$. First we multiply each term in equation (71) by $(\frac{|\xi_{l,i}|}{\xi_{min}})^{1/2}$ and then use the inequality (70) so that we have

$$
\|Bu_{GB}(x,t)\|_{L^2([0,T]\times\partial D)}^2 \preceq \frac{1}{\xi_{min}}\sum_{l,i,k}|c_{l,i,k}|^2.
\tag{77}
$$

Note that by differentiating $Bu_{GB}(x,t)$, we gain an extra coefficient $\xi_{l,i}$ for each beam and the others still keep bounded. More importantly, the property that the beam has Gaussian decay on the boundary $[0,T]\times\partial D$ is unchanged, so the inequality (77) can be adapted to the H^1 norm as follows:

$$
\|Bu_{GB}(x,t)\|_{H^1([0,T]\times\partial D)}^2 \preceq \frac{1}{\xi_{min}}\sum_{l,i,k}\xi_{l,i}^2|c_{l,i,k}|^2.
\tag{78}
$$

Now applying Lemma 5.4 and Lemma 5.3 yields the proof. ∎

6 Numerical results

In this section we will test our algorithm in 1-D and 2-D domains. Numerical simulations will be carried out for both constant and variable velocities. Note that the analytic solution may not be available for variable velocities. To calibrate our computed beam solutions, we obtain the "exact" solution by a fourth-order finite difference method [5] with a dense grid (up to 8192 points on each dimension) over the computational domain. The CFL condition is chosen to be $CFL = 0.5$, which is small enough to control the dispersion error of the solution. To identify significant beams, we choose the cut-off threshold ϵ to be 10^{-3}. All the errors are measured in the discrete relative L^2 norm.

6.1 One-dimensional domains

Let $D = [0, 0.5]$ and $N = 8192$. The initial conditions are given by:

$$
\begin{aligned}
f_1 &= 2\sin(\omega\pi x)\exp(-40(x - 0.25)^2);\\
f_2 &= 0.
\end{aligned}
\tag{79}
$$

The velocity changes in different cases. In order to confirm the convergence rate obtained by the analysis, we vary the main frequency ω of the initial conditions. Given the exact solution $u(x)$ and the Gaussian beam solution u_{GB} on the grid, the relative L^2 error is evaluated by the following formula:

$$
e_k = \frac{\sqrt{\frac{1}{N}\Sigma_{i=1}^N(u_i - u_{GBi})^2}}{\sqrt{\frac{1}{N}\Sigma_{i=1}^N u_i^2}}.
\tag{80}
$$

6.1.1 Case 1: Linear velocity

Example 1: Our first example is the wave equation with a linear velocity, where $V(x) = 1+0.5x$. Figure 3 gives the result for frequencies $\omega = 620$ and $\omega = 980$ at $t = 0.5$. The exact solution and the Gaussian beam solution are overlayed in these figures. As we can see, the differences between the two solutions are almost negligible. Figure 4 graphs the convergence rate by evaluating (80) in terms of different frequencies. The rate is approximately 0.5, which is in agreement with our analysis.

(a)   (b)
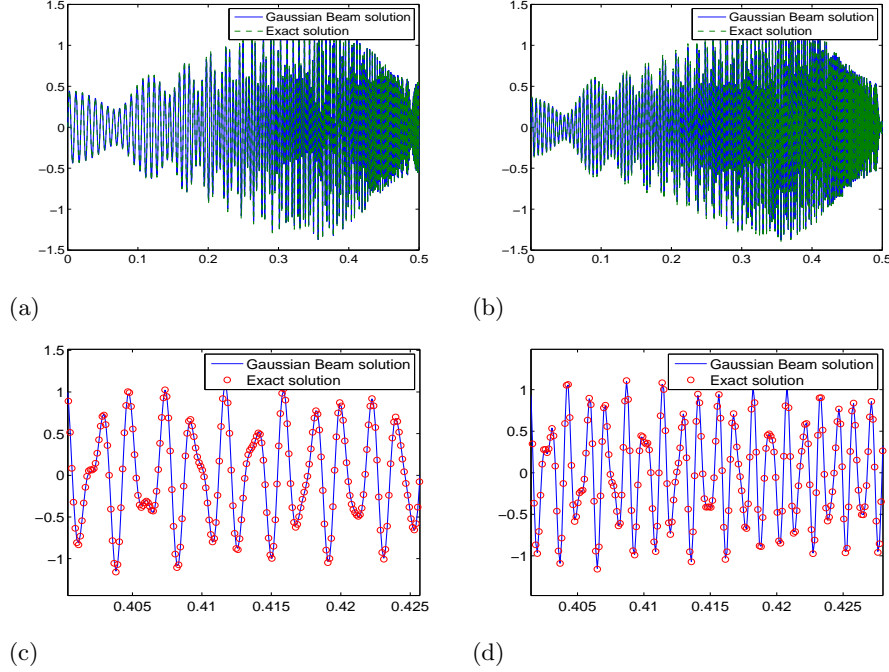
(c)   (d)
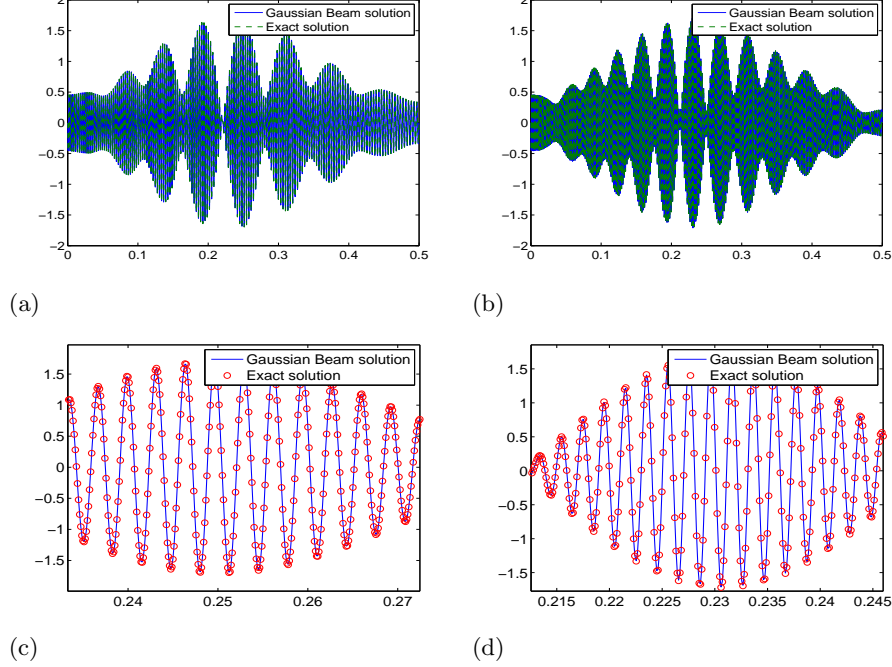
Figure 3: *Example 1. Linear model in 1D. (a) Comparison between the beam solution and exact solution at $\omega = 620$; (b) Comparison between the beam solution and exact solution at $\omega = 980$; (c) Windowed comparison between the beam solution and exact solution at $\omega = 620$; (d) Windowed comparison between the beam solution and exact solution at $\omega = 980$.*
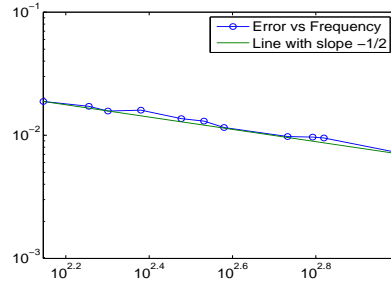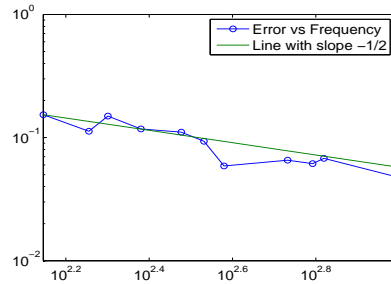

Figure 4: *Relative L^2 errors for linear velocity in Example 1*

Example 2: The second example has the same velocity and initial profile as Example 1,

but the initial time derivative is nonzero, which is defined as:

$$f_2 = \omega \sin(\omega \pi x).$$

Figure 5 gives the result for frequencies $\omega = 620$ and $\omega = 980$ at $t = 0.5$. The two solution are almost identical to each other. Figure 6 shows the convergence rate, which agrees with the analysis as well.

(a) (b) (c) (d)
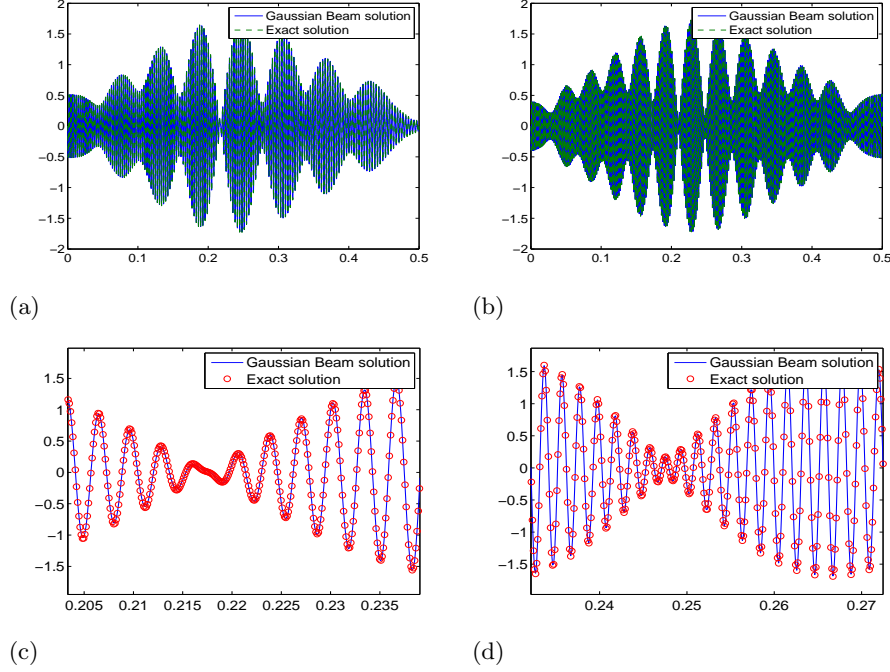
Figure 5: *Example 2. Linear model in 1D. (a) Comparison between the beam solution and exact solution at $\omega = 620$; (b) Comparison between the beam solution and exact solution at $\omega = 980$; (c) Windowed comparison between the beam solution and exact solution at $\omega = 620$; (d) Windowed comparison between the beam solution and exact solution at $\omega = 980$.*
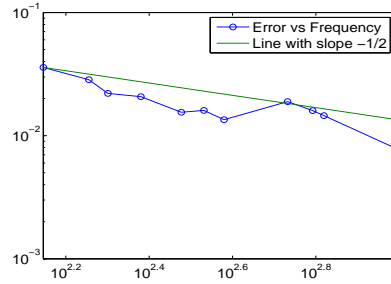
Figure 6: *Relative L^2 errors for linear velocity in Example 2*

6.1.2　Case 2: Sinusoidal velocity

Example 3: The velocity in this example is $V(x) = 1 + 0.5\cos(2\pi x)$. The initial conditions are given by equations (79). Figure 7 is the comparison between the Gaussian beam solution and the finite-difference solution at time $t = 0.5$ for frequencies $\omega = 620$ and $\omega = 980$, respectively. Figure 8 shows the convergence rate, and it agrees with the theoretical result.

The number of beams that has been launched in all these 1-D examples is around 1200. For instance, 1156 beams are launched for $\omega = 980$ in the sinusoid case, which accounts for approximately 28% of the total number of beams.

Figure 7: *Example 3. Sinusoidal model in 1D. (a) Comparison between the beam solution and exact solution at $\omega = 620$; (b) Comparison between the beam solution and exact solution at $\omega = 980$; (c) Windowed comparison between the beam solution and exact solution at $\omega = 620$; (d) Windowed comparison between the beam solution and exact solution at $\omega = 980$.*

Figure 8: *Relative L^2 errors for sinusoidal velocity in Example 3*

6.2 Two-dimensional rectangular domains

Consider the wave equation in the domain $[0, 0.5] \times [0, 0.5]$ for different velocities. Reflection condition for the Hessian is given by equation (30) when the beam hits the boundary. The domain is uniformly discretized by $N \times N = 2048 \times 2048$. Initial conditions for the first three of the following examples are given by:

$$f_1 = 2\sin(\omega\pi(x+y))\exp(-40((x-0.25)^2 + (y-0.25)^2)), \qquad (81)$$
$$f_2 = 0,$$

where ω will vary in order to verify the convergence rate. In particular, ω increases by 20 from 60 to 240. The computation stops at $t = 0.5$.

6.2.1 Case 1: Linear velocity

Example 4: The velocity is given by $V(x, y) = 1 + 0.5(x + y)$. Figures 9(a) and 9(b) show the exact solution and the Gaussian beam solution for $\omega = 180$, respectively. Figures 9(c) and 9(e) show the comparison for the slice at $x = 0.25$. Figures 9(d) and 9(f) show the comparison for the slice at $y = 0.125$. Figure 10 demonstrates the relative L_2 convergence rate, which agrees with the analysis. There are 36736 beams propagating in the computational domain at $\omega = 180$, which only accounts for 0.4% of the total number of beams.

6.2.2 Case 2: Sinusoidal velocity

Example 5: Consider $V(x, y) = 1 + 0.25\sin(2\pi(x + y))$. Figure 11(a) shows the exact solution for $\omega = 220$. The Gaussian beam solution for $\omega = 220$ is shown in Figure 11(b). Figures 11(c), 11(d), 11(e) and 11(f) compare the solutions for different slices. Figure 12 shows the convergence result based on the different frequencies, and it matches with the analysis very well.

6.2.3 Case 3: Sinusoidal velocity

Example 6: Consider $V(x, y) = 1 + 0.25\sin(2\pi x)\cos(2\pi y)$. Figure 13(a) shows the exact solution for $\omega = 220$. The multiscale Gaussian beam solution for $\omega = 220$ is shown in Figure 13(b). Figures 13(c), 13(d), 13(e) and 13(f) compare the solutions for different slices. Figure 14 shows the convergence result based on different frequencies.

6.2.4 Case 4: Sinusoidal velocity

Example 7: Consider $V(x, y) = 1 + 0.25\sin(2\pi x)\cos(2\pi y)$ with the following initial data:

$$f_1 = 2\sin(\omega\pi(x+y))x(0.5 - x)y(0.5 - y),$$
$$f_2 = \omega\cos(\omega\pi(x+y))x(0.5 - x)y(0.5 - y); .$$

Figure 15(a) shows the exact solution for $\omega = 220$. The multiscale Gaussian beam solution for $\omega = 220$ is shown in Figure 15(b). Figures 15(c), 15(d), 15(e) and 15(f) compare the solutions for different slices. Figure 16 shows the convergence result based on the different frequencies. It asymptotically satisfies the theoretical convergence rate.

6.3 Two-dimensional circular domains

We proceed to consider a circular domain which is centered at $(0.5, 0.5)$ with radius 0.25, and we embed this circular domain into the unit square. We discretize the unit square
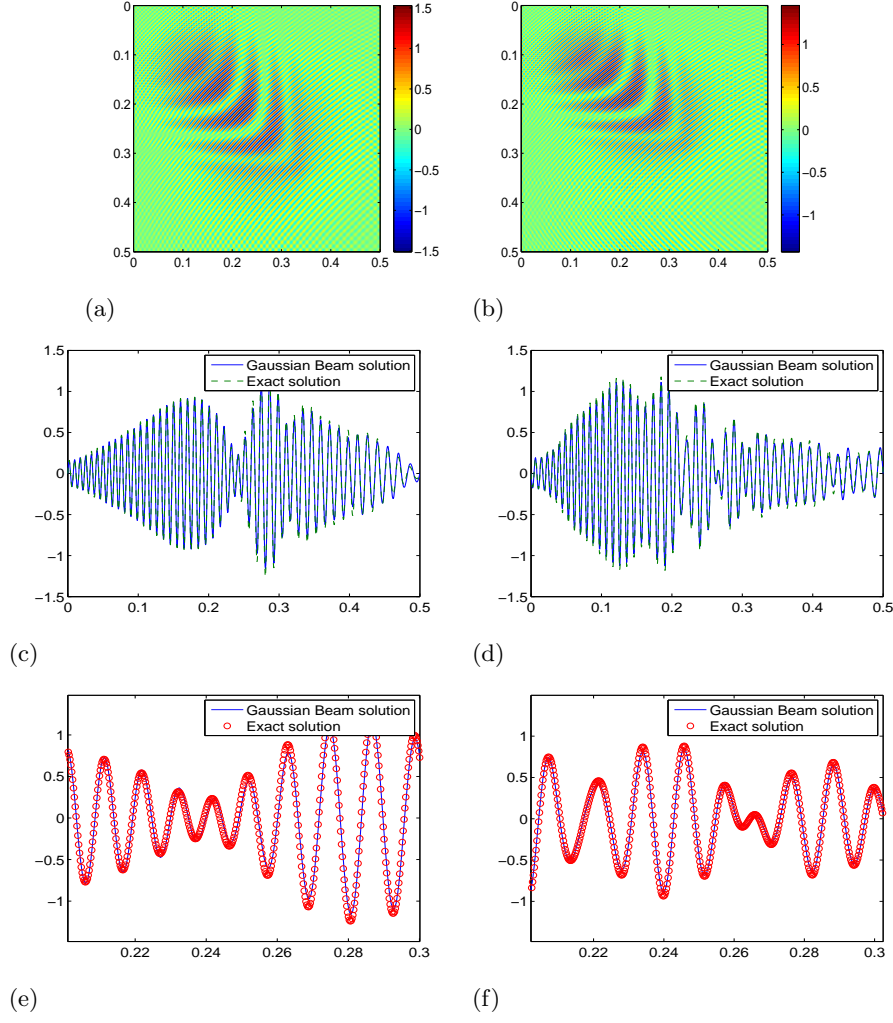
(a)

(b)

(c)

(d)

(e)

(f)

Figure 9: *Example 4. Linear model in 2D. (a) The exact solution at $\omega = 180$; (b) The beam solution at $\omega = 180$; (c) Comparison for the slice at $x = 0.25$; (d) Comparison for the slice at $y = 0.125$; (e)Windowed comparison for the slice at $x = 0.25$; (f)Windowed comparison for the slice at $y = 0.125$.*
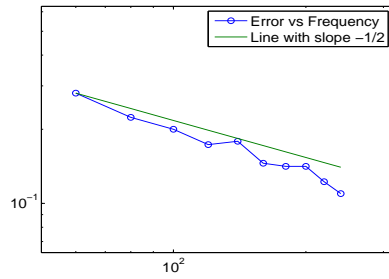

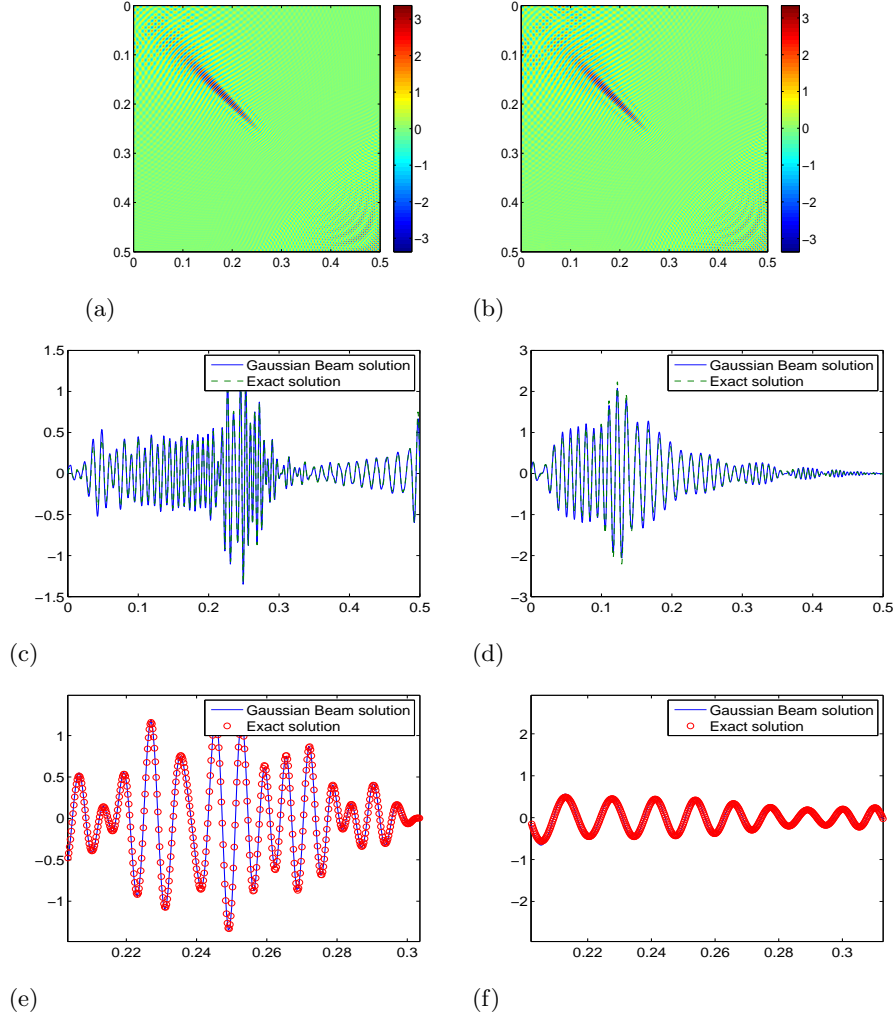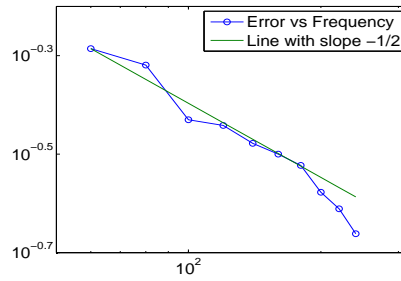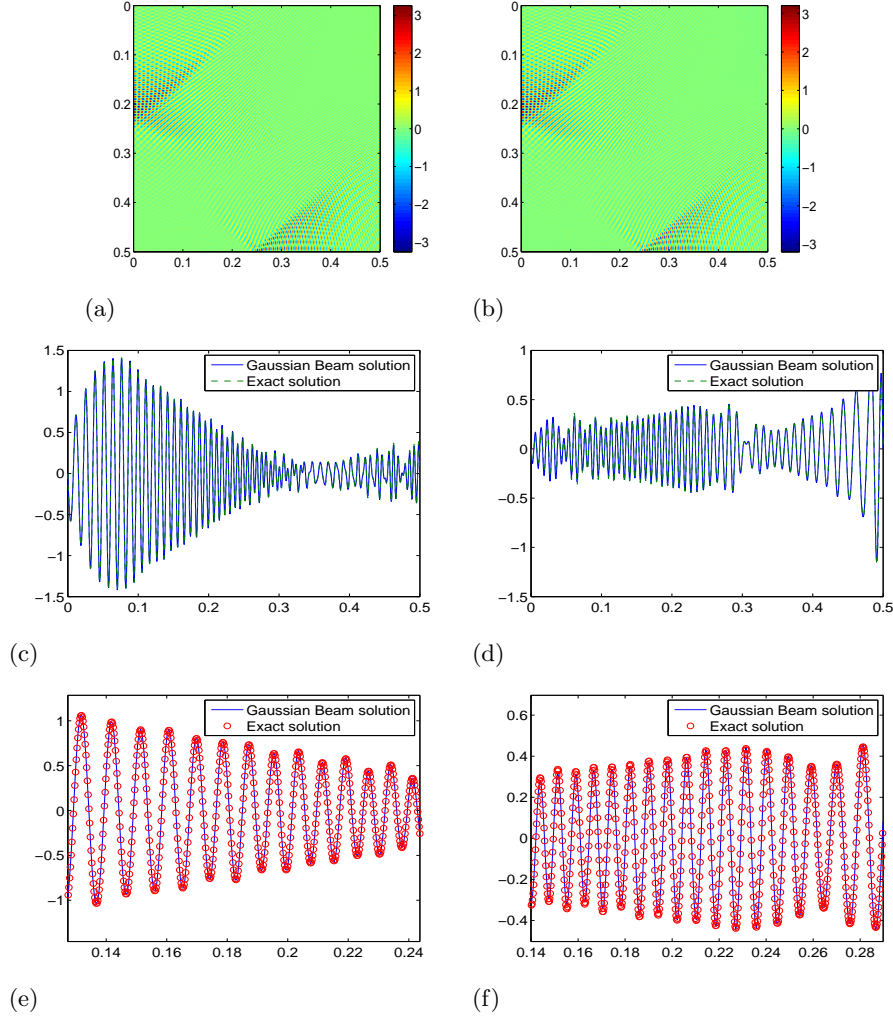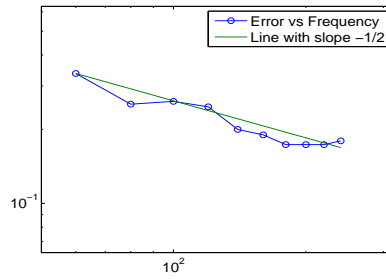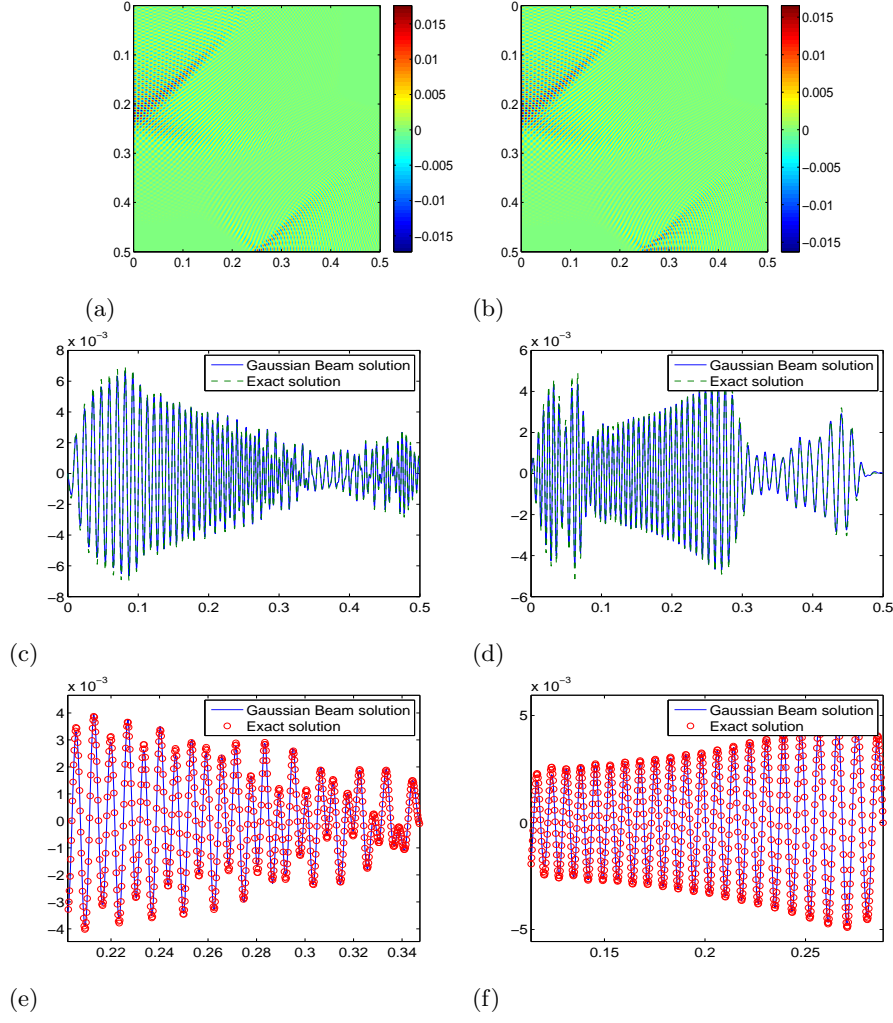Figure 10: *Relative L^2 errors for linear velocity in Example 4*

(a)

(b)

(c)

(d)

(e)

(f)

Figure 11: *Example 5. Sinusoidal model in 2D. (a) The exact solution at $\omega = 220$; (b) The beam solution at $\omega = 220$; (c) Comparison for the slice at $x = 0.25$; (d) Comparison for the slice at $y = 0.125$. (e) Windowed comparison for the slice at $x = 0.25$; (f) Windowed comparison for the slice at $y = 0.125$;.*
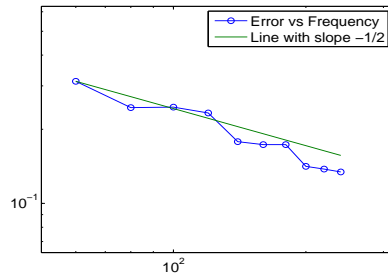

Figure 12: *Relative L^2 errors for sinusoidal velocity in Example 5*

Figure 13: *Example 6. Sinusoidal model in 2D. (a) The exact solution at $\omega = 220$; (b) The beam solution at $\omega = 220$; (c) Comparison for the slice at $x = 0.245$; (d) Comparison for the slice at $y = 0.245$. (e) Windowed comparison for the slice at $x = 0.245$; (f) Windowed comparison for the slice at $y = 0.245$;.*

Figure 14: *Relative L^2 errors for sinusoidal velocity in Example 6*

Figure 15: *Example 7. Sinusoidal model in 2D. (a) The exact solution at $\omega = 220$; (b) The beam solution at $\omega = 220$; (c) Comparison for the slice at $x = 0.20$; (d) Comparison for the slice at $y = 0.245$. (e) Windowed comparison for the slice at $x = 0.20$; (f) Windowed comparison for the slice at $y = 0.245$;.*

Figure 16: *Relative L^2 errors for sinusoidal velocity in Example 7*

26

uniformly by the grid of $N \times N = 2048 \times 2048$ mesh points. The computation stops at t=0.5. For the first three cases, we choose the initial conditions to be

$$f_1 = 2\sin(\omega\pi(x - 0.5))\sin((\omega + 20)\pi(y - 0.5))\exp(-40|x - 0.5, y - 0.5|),$$
$$f_2 = 0,$$

where $|x, y|$ denote the length of vector (x, y). To check the convergence rate, we evaluate ω at every 20 between 60 to 180. In order to get an accurate solution to compare with, we use a second-order accurate embedded boundary finite-difference method [7] to generate the "exact" solution.

6.3.1 Case 1: Constant velocity

Example 8: let $V(x, y) = 1$. Figure 17(a) gives the exact solution for $\omega = 180$. The Gaussian beam solution for $\omega = 180$ is given in Figure 17(b). Figures 17(c) and 17(e) and Figures 17(d) and 17(f) show the comparisons for the slices at $x = 0.45$ and $y = 0.47$, respectively. Figure 18 demonstrates the relative L_2 convergence rate.

6.3.2 Case 2: Sinusoidal velocity

Example 9: let $V(x, y) = 1 + 0.25\sin(2\pi(x + y))$. The result is shown in Figure 19. Figures 19(a) and 19(b) show the exact solution and the Gaussian Beam solution for $\omega = 180$, respectively. Figures 19(c) and 19(e) and Figures 19(d) and 19(f) compare the solutions for the slices at $x = 0.45$ and $y = 0.47$, respectively. Figure 20 plots the convergence result based on the four frequencies, and the convergence rate matches with the analysis result.

6.3.3 Case 3: Sinusoidal velocity

Example 10: let $V(x, y) = 1 + 0.25\sin(2\pi x)\cos(2\pi y)$. The result is shown in Figure 21. Figures 21(a) and 21(b) show the exact solution and the Gaussian Beam solution for $\omega = 180$, respectively. Figures 21(c) and 21(e) and Figures 21(d) and 21(f) compare the solutions for the slices at $x = 0.45$ and $y = 0.47$, respectively. Figure 22 plots the convergence result based on the four frequencies, and the convergence rate matches with the analysis result.

6.3.4 Case 4: Sinusoidal velocity

Example 11: Consider $V(x, y) = 1 + 0.25\sin(2\pi x)\cos(2\pi y)$, and the initial conditions are given by:

$$f_1 = 2\sin(\omega\pi(x - 0.5))\sin((\omega + 20)\pi(y - 0.5))\exp(-40|x - 0.5, y - 0.5|),$$
$$f_2 = \omega\cos(\omega\pi(x - 0.5))\cos((\omega + 20)\pi(y - 0.5))\exp(-40|x - 0.5, y - 0.5|).$$

The result is shown in Figure 23. Figures 23(a) and 23(b) show the exact solution and Gaussian Beam solution for $\omega = 180$ respectively. Figures 23(c) and 23(d) provide the comparison for the slices. Figure 24 plots the convergence result based on the different frequencies.

7   Conclusion

In this paper, we discuss how to construct global Gaussian Beam solutions in a bounded domain with multiple reflections. The initialization process is accomplished by the fast multiscale Gaussian wavepacket transform, which is fast and accurate in decomposing initial data. The theoretical analysis shows the convergence rate of the method. Numerical examples validate our algorithm. The convergence rate is verified in numerical examples.
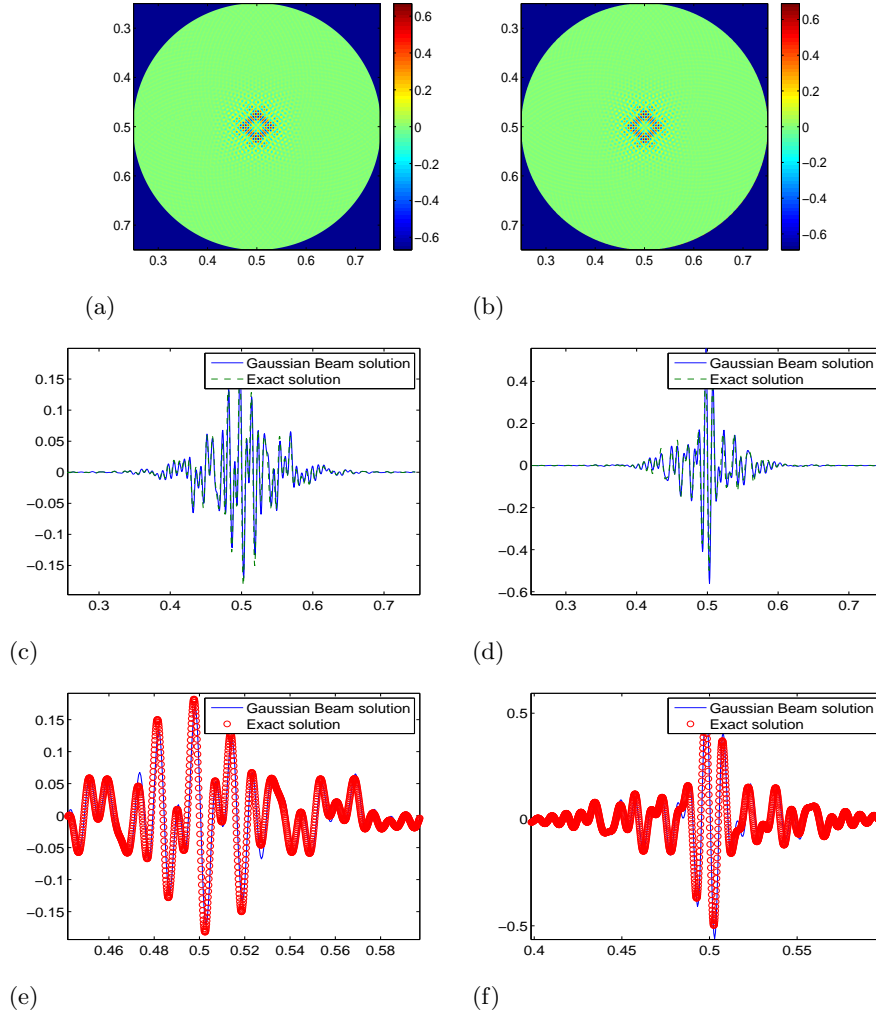
Figure 17: *Example 8. Constant model in 2D. (a) The exact solution at $\omega = 180$; (b) The beam solution at $\omega = 180$; (c) Comparison for the slice at $x = 0.45$; (d) Comparison for the slice at $y = 0.47$; (e) Windowed comparison for the slice at $x = 0.45$; (d) Windowed comparison for the slice at $y = 0.47$;*
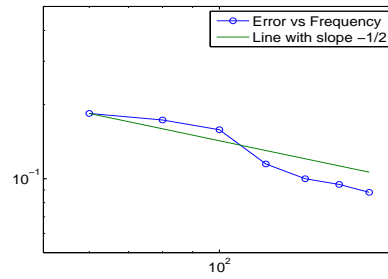

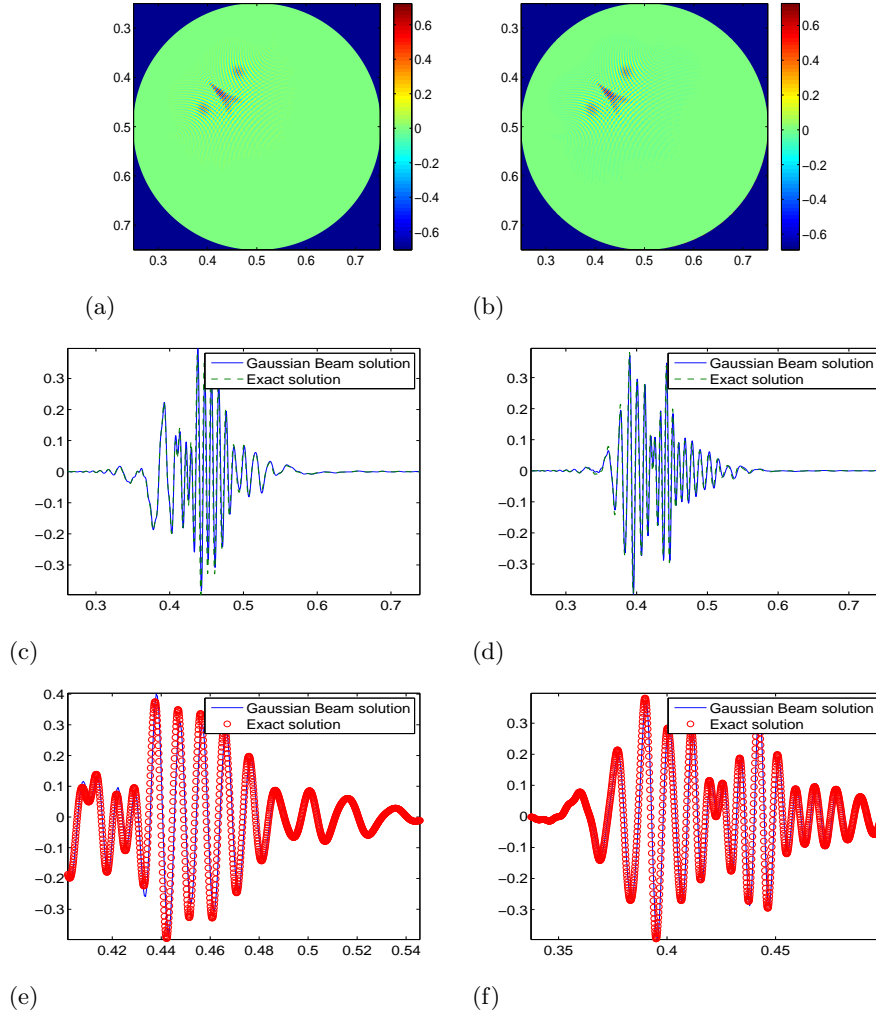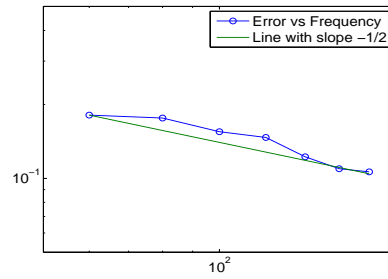Figure 18: *Relative L^2 errors for constant velocity in Example 8*

(a)

(b)

(c)

(d)

(e)

(f)

Figure 19: *Example 9. Sinusoidal model in 2D. (a) The exact solution at $\omega = 180$; (b) The beam solution at $\omega = 180$; (c) Comparison for the slice at $x = 0.45$; (d) Comparison for the slice at $y = 0.47$; (e)Windowed comparison for the slice at $x = 0.45$; (f) Windowed comparison for the slice at $y = 0.47$;*

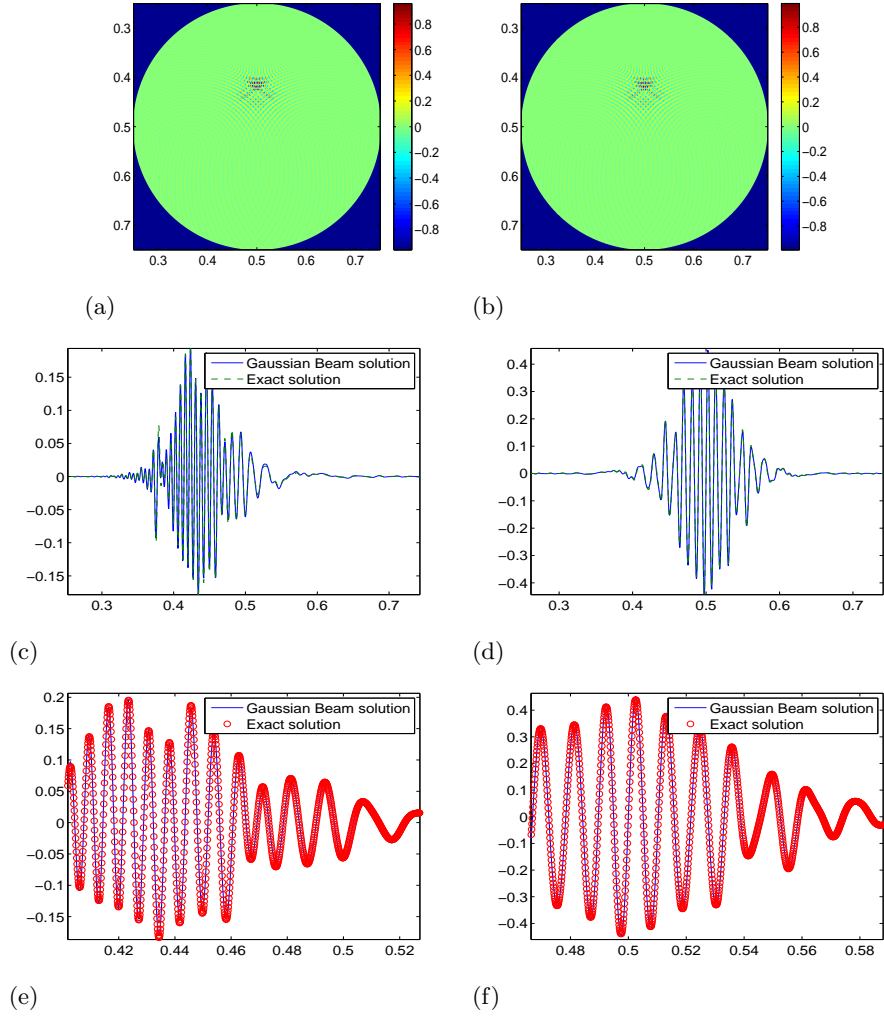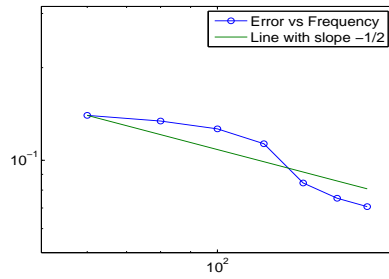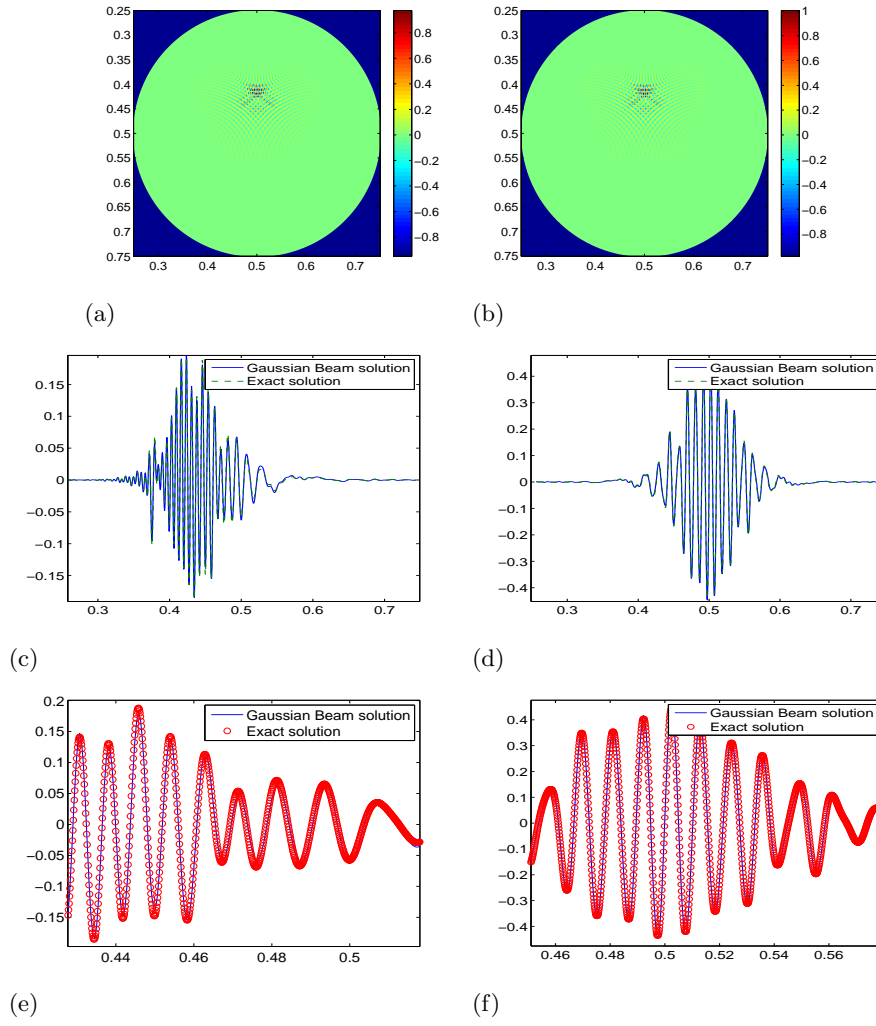Figure 20: *Relative L^2 errors for sinusoidal velocity in Example 9*

Figure 21: *Example 10. Sinusoidal model in 2D. (a) The exact solution at $\omega = 180$; (b) The beam solution at $\omega = 180$; (c) Comparison for the slice at $x = 0.45$; (d) Comparison for the slice at $y = 0.45$; (e)Windowed comparison for the slice at $x = 0.45$; (f) Windowed comparison for the slice at $y = 0.45$;*

Figure 22: *Relative L^2 errors for sinusoidal velocity in Example 10*

Figure 23: *Example 11. Sinusoidal model in 2D. (a) The exact solution at $\omega = 180$; (b) The beam solution at $\omega = 180$; (c) Comparison for the slice at $x = 0.45$; (d) Comparison for the slice at $y = 0.45$; (e)Windowed comparison for the slice at $x = 0.45$; (f) Windowed comparison for the slice at $y = 0.45$;*
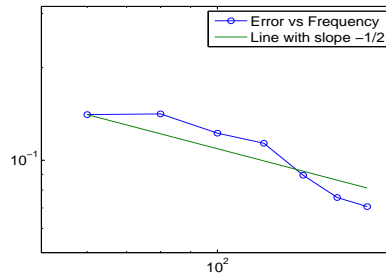

Figure 24: *Relative L^2 errors for sinusoidal velocity in Example 11*

Acknowledgement

References

[1] V. M. Babich and V. S. Buldyrev. *Asymptotic methods in short wave diffraction problems (in Russian)*. Nauka, Moscow, 1972.

[2] G. Bao, J. Qian, L. Ying, and H. Zhang. A convergent multiscale Gaussian-beam parametrix for the wave equation. *Commun. PDEs*, 38:92–134, 2013.

[3] S. Bougacha, J. Akian, and R. Alexandre. Gaussian beams summation for the wave equation in a convex domain. *Commun. Math. Sci.*, 7:973–1008, 2009.

[4] V. Cerveny, M. Popov, and I. Psencik. Computation of wave fields in inhomogeneous media-Gaussian beam approach. *Geophys. J. R. Astr. Soc.*, 70:109–128, 1982.

[5] G. Cohen. *Higher-order Numerical Methods for Transient Wave Equations*. Springer, 2001.

[6] N. Hill. Gaussian beam migration. *Geophysics*, 55:1416–1428, 1990.

[7] H. Kreiss and N. Petersson. A second-order accurate embedded boundary method for the wave equation with Dirichlet data. *SIAM J. Sci. Comput.*, 27:1141–1167, 2006.

[8] S. Leung and J. Qian. Eulerian Gaussian beam methods for Schrödinger equations in the semi-classical regime. *J. Comput. Phys.*, 228:2951–2977, 2009.

[9] S. Leung and J. Qian. The backward phase flow and FBI-transform-based Eulerian Gaussian beams for the Schrödinger equation. *J. Comput. Phys.*, 229:8888–8917, 2010.

[10] S. Leung, J. Qian, and R. Burridge. Eulerian Gaussian beams for high frequency wave propagation. *Geophysics*, 72:SM61–SM76, 2007.

[11] H. Liu, O. Runborg, and N. M. Tanushev. Error estimates for Gaussian beam superpositions. *Math. Comp.*, 82:919–952, 2013.

[12] V. P. Maslov. *The Complex WKB Method for Nonlinear Equations I: Linear theory*. Birkhauser Verlag, Basel, 1994.

[13] M. Motamed and O. Runborg. Taylor expansion and discretization errors in Gaussian beam superposition. *Wave Motion*, 47:421–439, 2010.

[14] A. Norris, B. S. White, and J. Schrieffer. Gaussian wave packets in inhomogeneous media with curved interfaces. *Proc. R. Soc. Lond. A*, 412:93–123, 1987.

[15] M. M. Popov. A new method of computation of wave fields using Gaussian beams. *Wave Motion*, 4:85–97, 1982.

[16] J. Qian and L. Ying. Fast Gaussian wavepacket transforms and Gaussian beams for the Schrödinger equation. *J. Comput. Phys.*, 229:7848–7873, 2010.

[17] J. Qian and L. Ying. Fast multiscale Gaussian wavepacket transforms and multiscale Gaussian beams for the wave equation. *SIAM J. Multiscale Modeling and Simulation*, 8:1803–1837, 2010.

[18] J. Ralston. Gaussian beams and the propagation of singularities. Studies in partial differential equations. MAA Studies in Mathematics, 23. Edited by W. Littman. pp.206-248., 1983.

[19] G. Russo and P. Smereka. The Gaussian wave packet transform: Efficient computation of the semi-classical limit of the Schrödinger equation. Part 1 Formulation and the one dimensional case. *J. Comput. Phys.*, 233:192–209, 2013.

[20] N. Tanushev, B. Engquist, and R. Tsai. Gaussian beam decomposition of high frequency wave fields. *J. Comput. Phys.*, 228:8856–8871, 2009.

[21] N. Tanushev, J. Qian, and J. Ralston. Mountain waves and Gaussian beams. *SIAM J. Multiscale Modeling and Simulation*, 6:688–709, 2007.

[22] A. Waters. A parametrix construction for the wave equation with low regularity coefficients using a frame of Gaussians. *Commun. Math. Sci.*, 9:225–254, 2011.

[23] D. Yin and C. Zheng. Gaussian beam formulations and interface conditions for the one-dimensional linear Schrödinger equations. *Wave Motion*, 48:310–324, 2011.